

# Development and Use of System Modeler 6DOF Flight Mechanics Model in Aircraft Conceptual Design

---

*Utveckling och Användning av System Modeler 6DOF  
Flygmekanik Modell i Konceptuell Design av Flygplan*

**Niko Erä-Esko**

Supervisor : Jorge Lovaco  
Co-Supervisor : Robert Hällqvist  
Co-Supervisor : Alexandra Oprea  
Examiner : Ingo Staack

External supervisor : Ankit Naik

## Upphovsrätt

Detta dokument hålls tillgängligt på Internet - eller dess framtida ersättare - under 25 år från publiceringsdatum under förutsättning att inga extraordinära omständigheter uppstår.

Tillgång till dokumentet innebär tillstånd för var och en att läsa, ladda ner, skriva ut enstaka kopior för enskilt bruk och att använda det oförändrat för ickekommersiell forskning och för undervisning. Överföring av upphovsrätten vid en senare tidpunkt kan inte upphäva detta tillstånd. All annan användning av dokumentet kräver upphovsmannens medgivande. För att garantera äktheten, säkerheten och tillgängligheten finns lösningar av teknisk och administrativ art.

Upphovsmannens ideella rätt innefattar rätt att bli nämnd som upphovsman i den omfattning som god sed kräver vid användning av dokumentet på ovan beskrivna sätt samt skydd mot att dokumentet ändras eller presenteras i sådan form eller i sådant sammanhang som är kränkande för upphovsmannens litterära eller konstnärliga anseende eller egenart.

För ytterligare information om Linköping University Electronic Press se förlagets hemsida <http://www.ep.liu.se/>.

## Copyright

The publishers will keep this document online on the Internet - or its possible replacement - for a period of 25 years starting from the date of publication barring exceptional circumstances.

The online availability of the document implies permanent permission for anyone to read, to download, or to print out single copies for their own use and to use it unchanged for non-commercial research and educational purpose. Subsequent transfers of copyright cannot revoke this permission. All other uses of the document are conditional upon the consent of the copyright owner. The publisher has taken technical and administrative measures to assure authenticity, security and accessibility.

According to intellectual property law the author has the right to be mentioned when their work is accessed as described above and to be protected against infringement.

For additional information about the Linköping University Electronic Press and its procedures for publication and for assurance of document integrity, please refer to its www home page: <http://www.ep.liu.se/>.

## Abstract

This thesis presents a tool for conceptual design of a traditional configuration aircraft by using a parametric six degrees of freedom (6DOF) flight mechanics model implemented in the Modelica Language using Wolfram System Modeler. Being first only able to model and simulate the uncontrolled flight of an aircraft with fixed mass and centre of gravity (CG), and requiring detailed aerodynamic parameters as an input, the 6DOF model is improved by developing new features to reduce the number of required inputs while also increasing the data output of the simulations.

First, the propulsion submodel is added with models for alternative propulsions to the existing model of turbofan engines. The energy and fuel consumption is also modelled for all propulsion types, and thus the aircraft model has no longer fixed mass properties, except for aircraft with electric propulsion. To further evaluate the fuel consumption for pre-defined flight missions with given flight speed, altitude and track angles, autopilots for a few different aircraft types are developed. Additionally, the 6DOF model is improved by establishing algebraic and statistical relationships between the aircraft geometric input parameters, aerodynamic coefficients and moments of inertia such that the values for the two last mentioned can be estimated inside the 6DOF model based on the minimum amount of design variables, geometric input parameters and aerodynamic properties of the 2D airfoils used in the wings.

Ultimately, the improved 6DOF model is evaluated and analysed in terms of its performance in initial weight estimation on aircraft conceptual design stage as well as in predicting the aerodynamic properties.

# Acknowledgments

I want to thank all my supervisors for their guidance and involvement in this thesis project. I would especially like to thank Wolfram MathCore for providing the opportunity and tools to do this thesis with a topic matching my interests in flight mechanics and modelling and simulation. Thank you also to their employees who helped me whenever I needed it. Lastly, I want to thank the Finnish education system for a stimulating education especially in mathematics and physics that eventually pushed me into higher education in engineering.

*Linköping, June 2022*

*Niko Erä-Esko*

# Nomenclature

## Abbreviations and Acronyms

Abbreviation	Meaning
6DOF	Six Degrees of Freedom
AC	Aircraft
CFD	Computational Fluid Dynamics
CG	Centre of Gravity
DASSL	Differential/Algebraic System Solver
LE	Leading edge
NACA	National Advisory Committee for Aeronautics
PID	Proportional-Integral-Derivative
USAF	United States Air Force

## Latin Symbols

Symbol	Description	Units
$a$	speed of sound	$[m\ s^{-1}]$
$\mathbf{a}$	linear acceleration vector	$[m\ s^{-2}]$
$AR$	aspect ratio	$[-]$
$b$	wing span	$[m]$
$BSFC$	brake-specific fuel consumption	$[kg\ W^{-1}\ s^{-1}]$
$c$	chord length	$[m]$
$C$	circumference	$[m]$
$c(y)$	local chord length at y-coordinate	$[m]$
$C_D$	drag coefficient	$[-]$
$C_f$	skin-friction drag coefficient	$[-]$
$C_L$	lift coefficient	$[-]$
$C_{l_\alpha}$	lift curve slope of 2D airfoil	$[rad^{-1}]$
$C_{L_\alpha}$	lift curve slope of 3D wing	$[rad^{-1}]$
$C_{l_{\delta_a}}$	control derivative coefficient for change in roll moment due to aileron deflection	$[rad^{-1}]$
$C_{l_p}$	stability derivative coefficient for change in roll moment due to roll rate	$[rad^{-1}]$
$e$	specific energy	$[J\ kg^{-1}]$
$E$	gross energy capacity; consumed energy	$[J]$
$\mathbf{F}$	force vector	$[N]$
$FF$	form factor	$[-]$
$h$	altitude; height	$[m]$
$i$	incidence angle	$[rad]$

Symbol	Description	Units
<b>I</b>	inertia tensor	$[kg\ m^2]$
$I_{xx}, I_{yy}, I_{zz}$	moments of inertia	$[kg\ m^2]$
$I_{xy}, I_{xz}, I_{yz}$	products of inertia	$[kg\ m^2]$
$k$	skin roughness value; sign for coefficient	$[m], [-]$
$K$	induced drag factor	$[-]$
$K_{C^{n_{\delta_a}}}$	empirical factor for estimating yaw due to aileron deflection	$[-]$
$l$	length	$[m]$
$L$	roll moment	$[N\ m]$
$m$	mass	$[kg]$
$M$	mach number; pitch moment	$[-], [N\ m]$
$n$	load factor; number of items	$[-]$
$N$	yaw moment	$[N\ m]$
$p$	roll rate; pressure	$[rad\ s^{-1}], [Pa]$
$P$	power	$[W]$
$q$	pitch rate; dynamic pressure	$[rad\ s^{-1}], [Pa]$
$Q$	interference factor	$[-]$
$r$	yaw rate	$[rad\ s^{-1}]$
$r_g$	radius of gyration	$[m]$
$Re$	reynolds number	$[-]$
$S$	area	$[m^2]$
$t$	time; thickness	$[s], [m]$
$T$	thrust, temperature	$[N], [K]$
$TR$	throttle ratio	$[-]$
$TSFC$	thrust-specific fuel consumption	$[kg\ N^{-1}\ s^{-1}]$
$U$	energy density	$[J\ m^{-3}]$
$v$	velocity	$[m\ s^{-1}]$
$V$	volume	$[m^3]$
$w$	width	$[m]$
$y$	y-coordinate	$[m]$
$z$	z-coordinate	$[m]$

## Greek Symbols

Symbol	Description	Units
$\alpha$	angle of attack	$[rad]$
$\alpha$	angular acceleration vector	$[rad\ s^{-2}]$
$\beta$	sideslip angle	$[rad]$
$\gamma$	flight path angle; adiabatic index	$[rad], [-]$
$\Gamma$	dihedral angle	$[rad]$
$\delta$	control actuator deflection; pressure ratio	$[rad], [-]$
$\epsilon$	downwash angle	$[rad]$
$\eta$	efficiency	$[-]$
$\theta$	pitch angle; temperature ratio	$[rad], [-]$
$\lambda$	taper ratio	$[-]$
$\Lambda$	sweep angle	$[rad]$
$\rho$	air density	$[kg\ m^{-3}]$

Symbol	Description	Units
$\sigma$	sidewash angle	[rad]
$\tau$	ratio of thickness-to-chord ratios at the tip and root	[-]
$\boldsymbol{\tau}$	torque vector	[N m]
$\phi$	roll angle	[rad]
$\psi$	yaw angle	[rad]

## Subscripts and superscripts

Abbreviation	Meaning
0	property values at sea-level / zero-lift conditions
a	ailerons
abs	seats abreast
ac	entire aircraft
AC	aerodynamic centre
alt	property value at altitude
avail	available
batt	battery system
cell	battery cell
CG	centre of gravity
ctrf	centre fuel tank
cutoff	cut-off value
des	design value
e	elevator
eff	effective
eng	engine
est	estimated value
exp	exposed (area)
fr	fuselage reference frame
FRP	fuselage reference plane
fuel	consumed fuel
fus	fuselage
HC	half chord
HT	horizontal tail
i	induced
lg	landing gear
max	maximum value
mech	power transmission of a powertrain
ML	maximum landing value
MTO	maximum take-off value
nac	nacelle
neg	negative
pax	passengers
PL	payload
prop	propeller
r	rudder
ref	reference value (area)

---

<b>Abbreviation</b>	<b>Meaning</b>
seat	airline seat
sys	systems installed onboard
T	throttle
tot	total, stagnation value
VT	vertical tail
w	main wing
wb	wing-body combination
wet	wetted (area)
wf	(one) wing fuel tank

---

# Contents

<b>Abstract</b>	<b>iii</b>
<b>Acknowledgments</b>	<b>iv</b>
<b>Nomenclature</b>	<b>viii</b>
<b>Contents</b>	<b>ix</b>
<b>List of Figures</b>	<b>xi</b>
<b>List of Tables</b>	<b>xii</b>
<b>1 Introduction</b>	<b>1</b>
1.1 Background . . . . .	1
1.2 Motivation . . . . .	1
1.3 Aim . . . . .	2
1.4 Delimitations . . . . .	3
<b>2 Theory</b>	<b>4</b>
2.1 Aircraft Conceptual Design . . . . .	4
2.2 Flight Mechanics . . . . .	4
<b>3 Method</b>	<b>6</b>
3.1 Autopilot . . . . .	6
3.2 Thrust Available and Fuel Consumption . . . . .	7
3.3 Algebraic and Statistical Relations Between Geometry and Aerodynamics . . . . .	9
3.3.1 Drag . . . . .	9
3.3.2 Lift . . . . .	12
3.3.3 Stall Behaviour . . . . .	12
3.3.4 Other Aerodynamic Coefficients . . . . .	14
3.4 Weight Estimation . . . . .	15
3.4.1 Fuselage . . . . .	15
3.4.2 Main Wing . . . . .	16
3.4.3 Tail . . . . .	16
3.4.4 Engines . . . . .	17
3.4.5 Fuel Tanks . . . . .	18
3.4.6 Battery . . . . .	18
3.4.7 Landing Gear . . . . .	19
3.4.8 Systems . . . . .	19
3.4.9 Payload . . . . .	20
3.5 Centre of Gravity Location . . . . .	20
3.5.1 Fuselage . . . . .	20
3.5.2 Wings . . . . .	21

3.5.3	Engines . . . . .	21
3.5.4	Fuel Tanks . . . . .	21
3.5.5	Battery . . . . .	23
3.5.6	Landing Gear . . . . .	23
3.5.7	Systems and Payload . . . . .	23
3.6	Inertia Tensor . . . . .	23
3.6.1	Engines . . . . .	23
3.6.2	Fuel Tanks . . . . .	24
3.6.3	Battery . . . . .	24
3.6.4	Landing Gear . . . . .	25
3.6.5	Payload . . . . .	25
3.6.6	Products of Inertia . . . . .	25
3.7	The Use of the Model in Aircraft Sizing . . . . .	26
3.8	Verification and Validation . . . . .	28
<b>4</b>	<b>Results</b>	<b>30</b>
4.1	Sizing . . . . .	30
4.2	Verification and Validation . . . . .	32
<b>5</b>	<b>Discussion</b>	<b>35</b>
5.1	Method . . . . .	35
5.1.1	Autopilot . . . . .	35
5.1.2	Fuel Consumption . . . . .	35
5.1.3	Algebraic and Statistical Relations Between Geometry and Aerodynamics	35
5.1.4	Mass and Inertia . . . . .	36
5.1.5	Verification and Validation and the Use of the Model in Aircraft Sizing .	37
5.2	Results . . . . .	37
5.2.1	Aircraft Sizing . . . . .	37
5.2.2	Verification and Validation . . . . .	37
<b>6</b>	<b>Conclusions</b>	<b>39</b>
	<b>Bibliography</b>	<b>40</b>
<b>A</b>	<b>Appendices</b>	<b>43</b>
A.1	Wing Coordinates . . . . .	43
A.2	Moment of Inertia Estimation for Wings and Fuselage . . . . .	46

# List of Figures

1.1	V-model adapted for aircraft design. [3]	2
2.1	Sign convention for control surface deflections and body frame axes with body angular velocities and moments.	5
3.1	Autopilot architecture.	7
3.2	$C_L$ vs. $\alpha$ curves showing the constraints defining the second order functions to model stall in the library.	13
3.3	Definitions for a sinus function to model $C_D$ vs. $\alpha$ with an example showing the curve for wing with $C_{D_{max}} = 1.2$ .	14
3.4	Curve chart for estimating $K_{C_{n_{\delta_a}}}$	15
3.5	Reference point from which the coordinates of the origin of components are measured from.	20
3.6	Dimensions and CG locations of the wing and centre tanks.	22
3.7	Mission profile from JFK to LHR and to diversion airport AMS.	27
3.8	Suggested aircraft sizing flowchart to be used with the Aircraft Library.	28
4.1	Fuel level as a fraction of the total tank volume and demand for throttle from autopilot.	31
4.2	Constrained variables of dynamic pressure and load factor with their limits.	31
5.1	Fuselage reference point and $c_{mean,w}$ leading edge which is used to define the position of the tail.	36
A.1	The position of the main wing origin.	43

# List of Tables

3.1	Standard passenger and baggage weights. [29]	20
3.2	CG locations for fuselage.	20
3.3	CG locations for wings.	21
3.4	Initial design variables and constraints for the aircraft design to be sized.	26
4.1	Deviations from the obtained aircraft total mass and flight trajectory variables using DASSL solver with a tolerance of $1 \text{ e-}6$ .	32
4.2	Validation of the aerodynamic coefficients against USAF DATCOM Digital Program results.	33
4.3	Validation of the mass properties against known values.	34



# 1 Introduction

## 1.1 Background

This thesis work builds upon a parametric 6DOF flight mechanics model developed by Wolfram MathCore and implemented in the Modelica Language using Wolfram System Modeler and planned to be released later in 2022. The model is referred to as the Aircraft Library later in this work. Prior to this work, the library was able to simulate the flight of a conventional configuration rigid-aircraft for which all aerodynamic and mass properties were known. The library included a model of the atmosphere according to the U.S. Standard Atmosphere [1], which had an influence on the aerodynamic forces and the thrust output of the simplified turbofan submodel implemented to the library.

In order to enable the library to be used in aircraft conceptual design, the library is to be enhanced with methods to derive the aerodynamic and mass properties based on the aircraft geometry and some selected design variables. Thus, the number of required user input parameters to model the properties of an aircraft in early design phases is decreased.

## 1.2 Motivation

There are many tools available for aircraft conceptual design for prediction of aerodynamic coefficients and stability and control derivatives of an aircraft with a given geometry. One such tool, the United States Air Force (USAF) DATCOM Digital program, was used for the validation of the obtained aerodynamic coefficients in this work. Other tools, such as the Open VSP developed by NASA, can also be used to generate the geometry of the aircraft design in addition to predict its aerodynamic performance.

With the predicted aerodynamic coefficients and stability and control derivatives from these tools, it can indeed be shown whether the aircraft design is stable, whether it can generate enough lift and the magnitude of the drag force in a spectrum of flight altitudes and velocities. However, modelling and deriving the aerodynamic forces in complicated dynamic states, e.g. when the aircraft starts to pitch up while also rolling to the right and yawing to the left with the consequent induced angles of attack and sideslip angle is not possible with these tools. Combining the models for aerodynamic coefficients and stability and control derivatives with a 6DOF rigid-aircraft model with a simulation gives all that data in addition to visualising the resulting trajectory of the aircraft.

That being said, bringing the 6DOF flight mechanics model with simulation capability to the aircraft conceptual design enables testing the performance of the aircraft design directly for any given flight path considering also the dynamic effects. Consequently, the workflow from aircraft geometry and design variables to detailed performance analysis in aircraft conceptual design can all be done in one tool.

Another aspect to why it is important to involve simulations early in the aircraft design process comes from the systems engineering perspective on aircraft design. In systems engineering, the development process is commonly conducted by following the V-model, shown in Fig. 1.1, in which the design process is divided into decomposition and integration phases. In aircraft design, both phases move vertically between aircraft level and component level. The aircraft design is subject to testing in each phase and on each level. Having a decent 6DOF simulator involving multiple disciplines on the aircraft level of the decomposition phase provides a versatile testing tool for checking how the requirements are met with a more holistic perspective. [2][3]

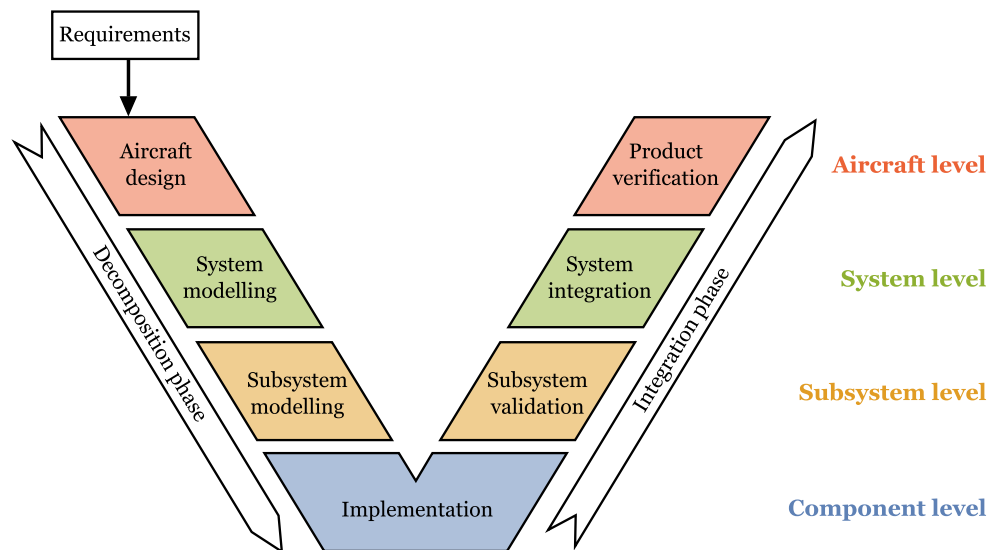


Figure 1.1: V-model adapted for aircraft design. [3]

### 1.3 Aim

The aim of this work is to develop and test a tool for aircraft conceptual design that involves simulation with a 6DOF flight mechanics model. The following six objectives are used to achieve the aim of this work:

1. Enable controlling of an arbitrary aircraft design for an arbitrary flight mission.
2. Improve the Aircraft Library by implementing empirical relations to estimate the aerodynamic coefficients and mass properties based on as few user input parameters on aircraft geometry and other design variables as possible, and by also considering the air compressibility effects for the aerodynamic coefficients.
3. Create a model for considering stall for the main wing and horizontal tail.
4. Create models for other propulsion types besides the turbofan model, and include the air compressibility effects into the propulsion models.
5. Use and test the improved Aircraft Library in aircraft sizing.
6. Compare the obtained aerodynamic coefficients and mass properties of existing aircraft with known or estimated values through other tools.

## 1.4 Delimitations

In this work, many new features were added to the library at the expense of their scope. These limitations include modelling only the subsonic and transsonic regimes below Mach 1. As a matter of fact, the current model experiences singularities at Mach 1, leading to numerical issues hence the resultant values of the aerodynamics properties become unreliable due to effects related to the formation of shock waves. Furthermore, despite the availability of the transsonic equations for estimating the aerodynamic coefficients, they were not always used due to their complexity and their need for adding more user input parameters on the aircraft geometry. When it comes to the flight mechanics, the effects from linear and angular accelerations are neglected.

In addition to the lack of high-lift devices and air brakes, the control actuators are also simplified by having no differential deflection of the ailerons but they are always deflected with equal and opposite angles, and the horizontal tail is not trimmable but with fixed incidence angle. The wing geometry is simplified to one tapered section with constant incidence angle with no spanwise twist.

Another domain that is not considered is disturbances or movement in the atmosphere, i.e. the atmospheric properties at the same altitude are invariable with time and there are no winds gusts or jet streams that would require modelling unsteady aerodynamics. The flight environment is further simplified by applying a non-rotating flat earth model. Additionally, with regard to the aircraft model, the aeroelasticity is not modelled in this work with the aircraft being considered as a rigid body.



## 2 Theory

In this chapter, the main disciplines of the theoretical framework of the thesis work are described. Additionally, the sign conventions used in this work are presented.

### 2.1 Aircraft Conceptual Design

The aircraft design process usually starts with the assessment of the requirements from customers, contractors and airworthiness authorities, that ideally together with new concept ideas define the span of the design space [4][5]. During aircraft conceptual design, the design space is explored and eventually narrowed down to one or few designs. Traditionally, the aircraft conceptual design has been carried out with static low-level statistical and empirical methods to evaluate the performance and the fulfillment of the requirements of the design. The validation of the concept through simulations has usually been conducted at the following design phase, namely the preliminary design phase. [6][7]

Along with the advancements in computational power, the methodology in aircraft conceptual design is shifting towards higher fidelity simulation based tools [8][6]. Thus, the model validation with simulation can already be involved during the aircraft conceptual design process, possibly as a part of an automated process to optimise the design.

### 2.2 Flight Mechanics

Flight mechanics is a broad term including a number of different disciplines, but in this work the definition by Hull [9] is used. He defines flight mechanics as the analysis of aircraft motion using the Newton-Euler first ( $\mathbf{F} = m \mathbf{a}$ ) and second ( $\boldsymbol{\tau} = \mathbf{I} \boldsymbol{\alpha}$ ) laws of motion for a rigid body. The complete set of rigid-body 6DOF equations of motion are solved in a frame fixed to the aircraft, hereinafter referred to as body frame. However, the body frame is unsuitable for describing the trajectory of the aircraft. Thus, the inertial frame fixed to the non-rotating flat earth model is used for solving the aircraft position and orientation. During a simulation, the aircraft differential equations of motion are numerically integrated to solve for the flown trajectory. [9][10]

Once the aircraft is airborne, the only forces acting on it other than the gravitational force are the aerodynamic forces and thrust. Thus, the forces and moments causing the linear and

angular motions in the aircraft equations of motion are solely consisting of them. The terms defining the couplings between the different motions along and around the three body axes are called stability derivatives, and they are derived from the aerodynamic coefficients, mass properties and geometry of the aircraft. They define for example roll moment ( $L$ ) due to yaw rate ( $r$ ) as the different sides of the main wing are experiencing different amount of lift due to their different velocities through air.

The contribution to the aircraft motion by the deflection of the control actuators is defined by control derivatives, which are derived from the geometry and location of the control actuators. The notation of control actuators and the sign convention for control surface deflections, body angular velocities and moments of Nelson [10] are used here, and they are shown in Fig. 2.1.

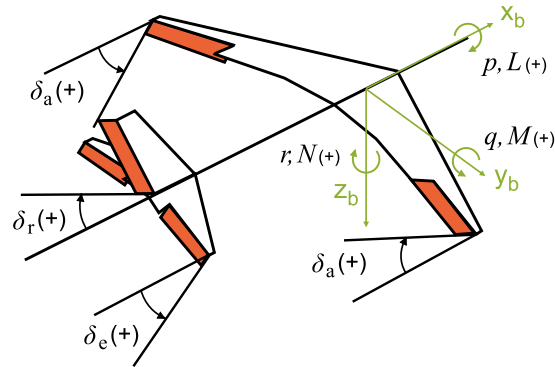


**Figure 2.1:** Sign convention for control surface deflections and body frame axes with body angular velocities and moments.

Not all stability and control derivatives need to be derived when using the physical modelling environment as some of their effects on the motion of the aircraft emerge automatically when the aerodynamic forces can be applied locally for each component with the correct lever arm. For example, if a downward force at the horizontal tail is applied due to a negative deflection of the elevator, the physical model automatically generates a corresponding positive pitching moment ( $M$ ) due to the location of the applied force. Consequently, deriving a value for the control derivative for pitch moment ( $q$ ) due to elevator deflection is unnecessary.

In theory, the need for deriving values for all stability and control derivatives could be removed entirely in physical modeling if all aerodynamic forces would be modelled with local dynamic pressure values instead of global values throughout the aircraft, including at different spanwise locations on the wing surfaces. This would naturally increase the computational cost compared to using the stability and control derivatives.



## 3 Method

The primary aim of this project was to enhance the Aircraft Library such that the aerodynamic and mass properties are estimated based on the aircraft geometry and some key design variables of the aircraft design given by the user and also by considering nonlinear effects due to air compressibility and stall. Eventually, the library would also be able to simulate the controlled flight of an aircraft design for a given flight mission. This chapter presents the used methodology to estimate the aerodynamic and mass properties from the user input parameters and how aircraft designs are controlled during a simulation. Moreover, the model verification and validation methods and an example case in using the library in aircraft sizing are presented.

### 3.1 Autopilot

An autopilot was built into the Aircraft Library that translates the flight trajectory variables, i.e. flight speed ( $v_{\text{tot}}$ ), altitude ( $h$ ) and track, that are used to define a flight mission, into control actuator commands, i.e. elevator deflection ( $\delta_e$ ), aileron deflection ( $\delta_a$ ), rudder deflection ( $\delta_r$ ) and throttle position ( $\delta_T$ ). The block diagram of the autopilot is shown in Fig 3.1.

The altitude is controlled by  $\delta_e$  with an inner feedback loop for controlling the pitch angle ( $\theta$ ), and thus having two PID-controllers in series. Similarly, track is controlled by  $\delta_a$  with an inner feedback loop for controlling the roll angle ( $\phi$ ) with two PID-controllers.  $v_{\text{tot}}$  is controlled by  $\delta_T$  with only one PID-controller and one feedback loop.  $\delta_r$  is used to hold the sideslip angle ( $\beta$ ) at zero with constant zero reference  $\beta$  input signal. Thereby, the autopilot has six PID-controllers that are to be tuned for different aircraft.

An automatic method for tuning all the 18 control gains of the six PID-controllers for any given aircraft became a demanding challenge, as the attempts to create a linearised model between the control actuator inputs and the motion of the aircraft failed. Thus, the tuning was done manually for different aircraft types. Experimenting on which factors of an aircraft affect the most on the dynamics between the control actuator inputs and flight trajectory variables showed the biggest effect from aircraft mass and propulsion type. As these parameters can generally be considered to be coupled, i.e. piston and electric engines are typically found in light aircraft whereas turboprop engines are found in mid-sized aircraft and turbofans in larger aircraft, four different autopilots were manually tuned for

these propulsion types. Different autopilots were made for electric and piston engines despite them occurring in similar size aircraft as the performance between the two engine types differ to a large extent in higher altitudes, as the equations in Sec. 3.2 show.

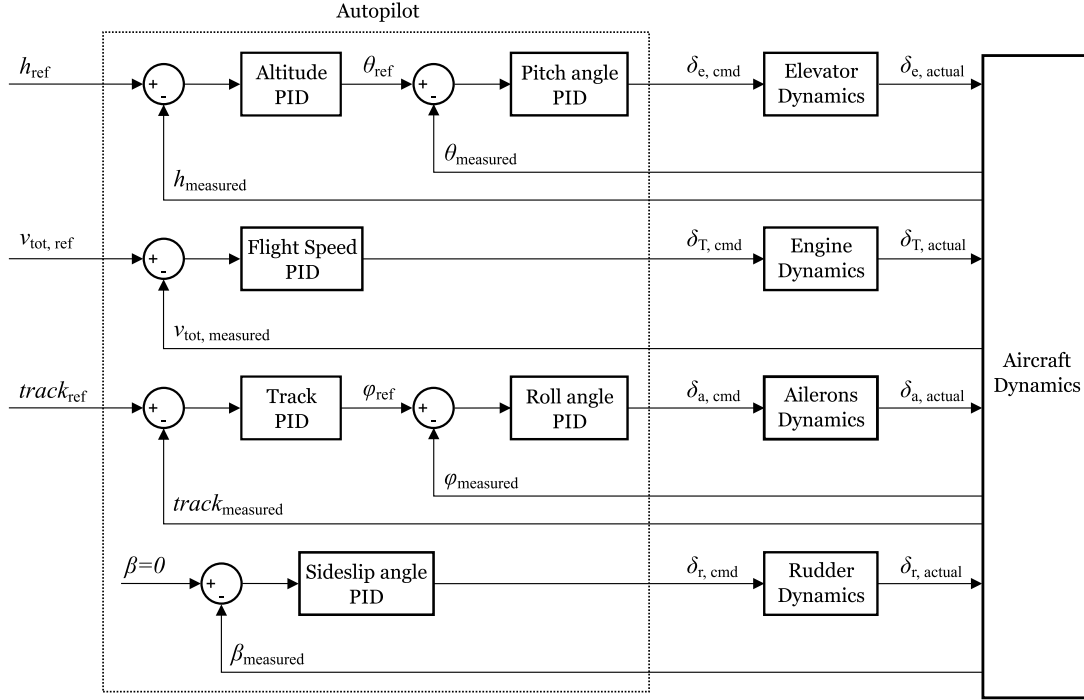


Figure 3.1: Autopilot architecture.

### 3.2 Thrust Available and Fuel Consumption

In the Aircraft Library, the produced net thrust of an engine ( $T_{net}$ ) is the product of thrust available ( $T_{avail}$ ) and  $\delta_T$  signal after engine dynamics, namely the  $\delta_{T, actual}$ . For turbofan and turbojet engines,  $T_{avail}$  is a function of air pressure at altitude ( $p_{alt}$ ), air temperature at altitude ( $T_{alt}$ ), Mach number ( $M$ ) and the static thrust at sea level ( $T_{static}$ ). For piston and turboprop engines, the performance is described by their maximum produced power at sea level ( $P_0$ ), which is used together with air density at altitude ( $\rho_{alt}$ ) to solve for the power available ( $P_{avail}$ ). The  $P_{avail}$  of electric engines does not vary over  $h$ , and thus their  $P_{avail}$  equals always  $P_0$  [11]. For piston, turboprop and electric engines, the  $T_{avail}$  was solved as a function of  $P_{avail}$ :

$$T_{avail} = \frac{P_{avail}}{v_{tot}} \eta_{prop} \eta_{mech} \quad (3.1)$$

where  $\eta_{prop}$  and  $\eta_{mech}$  are propeller and power transmission efficiencies, respectively. Their values were simplified to have constant values that are given by the user as parameters.

$P_{avail}$  at altitude for piston engines was solved through the relation given in [11]:

$$P_{avail} = P_0 \frac{\frac{\rho_{alt}}{\rho_0} - 0.117}{0.883} \quad (3.2)$$

For  $P_{avail}$  of turboprops, the relation given in reference [12] was used:

$$P_{avail} = P_0 \left( \frac{\rho_{alt}}{\rho_0} \right)^{0.7} \quad (3.3)$$

For turbofan and turbojet engines, there are two equations for solving  $T_{avail}$  depending on whether the temperature ratio ( $\theta$ ) is below or above the throttle ratio ( $TR$ ) that is an

engine design parameter dependent on engine design Mach number ( $M_{\text{des,eng}}$ ) and design altitude ( $h_{\text{des}}$ ). The values of  $\theta$  and  $TR$  are defined by the equations given in [11]:

$$\theta = \frac{T_{\text{tot}}}{T_0} = \frac{T_{\text{alt}}}{T_0} \left( 1 + \frac{\gamma - 1}{2} M^2 \right) \quad (3.4)$$

$$TR = \frac{T_{\text{des}}}{T_0} \left( 1 + \frac{\gamma - 1}{2} M_{\text{des,eng}}^2 \right) \quad (3.5)$$

where  $T_{\text{des}}$  is the temperature at  $h_{\text{des}}$  according to the U.S. Standard Atmosphere, and  $T_{\text{tot}}$  is the stagnation temperature. Thereby, two equations given in reference [11] were used to solve for  $T_{\text{avail}}$  of turbofan engines:

$$T_{\text{avail}} = \begin{cases} T_{\text{static}} \delta (1 - 0.49 \sqrt{M}) & \theta \leq TR \\ T_{\text{static}} \delta \left[ 1 - 0.49 \sqrt{M - \frac{3(\theta - TR)}{1.5 + M}} \right] & \theta > TR \end{cases} \quad (3.6)$$

where  $\delta$  is the pressure ratio at altitude and is defined by the relation between the stagnation and static pressures [11]:

$$\delta = \frac{p_{\text{tot}}}{p_0} = \frac{p_{\text{alt}}}{p_0} \left( 1 + \frac{\gamma - 1}{2} M^2 \right)^{\frac{\gamma}{\gamma - 1}} \quad (3.7)$$

For turbojet engines, two equations for solving  $T_{\text{avail}}$  given in reference [11] were used:

$$T_{\text{avail}} = \begin{cases} 0.8 T_{\text{static}} \delta (1 - 0.16 \sqrt{M}) & \theta \leq TR \\ 0.8 T_{\text{static}} \delta \left[ 1 - 0.16 \sqrt{M - \frac{24(\theta - TR)}{(9 + M)\theta}} \right] & \theta > TR \end{cases} \quad (3.8)$$

By using these equations for turbofan and turbojet engines, the air compressibility and altitude effects for engine performances are accounted for.

For calculating the fuel consumption ( $m_{\text{fuel}}$ ) of turbofan and turbojet engines, a new parameter for thrust-specific fuel consumption ( $TSFC$ ) was introduced to the model.  $TSFC$  is multiplied by  $T_{\text{net}}$  of an engine to get fuel burn rate which is integrated over time ( $t$ ) to determine fuel consumption:

$$m_{\text{fuel}} = \int T_{\text{net}} TSFC dt \quad (3.9)$$

For piston and turboprop engines, the brake-specific fuel consumption ( $BSFC$ ) was introduced as the parameter to calculate their fuel consumption. In order to get the fuel burn rate,  $T_{\text{net}}$  is first multiplied by  $v_{\text{tot}}$  to get the net propulsive power produced by the engine ( $P_{\text{net}}$ ). However, the power in  $BSFC$  refers to the generated shaft power of the engine rather than  $P_{\text{net}}$  [13]. Thus, the  $P_{\text{net}}$  signal is first divided by  $\eta_{\text{prop}}$  and  $\eta_{\text{mech}}$  to get the gross power ( $P_{\text{gross}}$ ) which is then multiplied by  $BSFC$ . Similarly, that signal is integrated over time to get the fuel consumption of piston and turboprop engines:

$$m_{\text{fuel}} = \int P_{\text{gross}} BSFC dt = \int \frac{P_{\text{net}}}{\eta_{\text{prop}} \eta_{\text{mech}}} BSFC dt = \int \frac{T_{\text{net}} v_{\text{tot}}}{\eta_{\text{prop}} \eta_{\text{mech}}} BSFC dt \quad (3.10)$$

For electric engines, the  $P_{\text{gross}}$  signal is integrated over time to get the consumed energy ( $E$ ):

$$E = \int P_{\text{gross}} dt = \int \frac{P_{\text{net}}}{\eta_{\text{prop}} \eta_{\text{mech}}} dt = \int \frac{T_{\text{net}} v_{\text{tot}}}{\eta_{\text{prop}} \eta_{\text{mech}}} dt \quad (3.11)$$

### 3.3 Algebraic and Statistical Relations Between Geometry and Aerodynamics

Prior to this work, the Aircraft Library required multiple aerodynamic coefficients from the user, that also had constant values during simulations regardless of the Mach number and Reynolds number. The aim was to establish relations between the aircraft geometry and aerodynamic coefficients and take the compressibility effects into account for lift and drag coefficients. Additionally, a model for stall behaviour for the main wing and horizontal tail was created. Eventually, the list of required aerodynamic coefficients as an input by the user was reduced to the properties of the 2D airfoils of each wing surface.

#### 3.3.1 Drag

As the lift-induced drag coefficient ( $C_{D,i}$ ) estimation was already implemented on the model, and the wave drag is omitted as supersonic regime is not modelled, only the parasite drag was to be estimated to the model, for which the component buildup method was used as presented by Raymer [5]. The method estimates the parasite drag coefficient ( $C_{D,0}$ ) for each component (c) individually:

$$C_{D,0,c} = \frac{C_{f,c} FF_c Q_c S_{wet,c}}{S_{ref,w}} \quad (3.12)$$

where  $C_f$  is flat-plate skin-friction drag coefficient,  $FF$  is form factor representing the pressure drag contribution and interference factor  $Q$  estimates the interference effects due to the component [5].  $S_{wet}$  is the wetted area of the component and  $S_{ref,w}$  is the main wing reference area.

There are two equations for  $C_f$  depending on whether the flow over the component is laminar or turbulent. For nacelles and the fuselage, completely turbulent flow was assumed over them, whereas for each wing (main wing, horizontal and vertical tail), the flow was assumed 10 % laminar and 90 % turbulent. Thus, the wings had a corresponding weighted average of the two equations for  $C_f$  [5]:

$$\text{Laminar: } C_f = \frac{1.328}{\sqrt{Re}} \quad (3.13)$$

$$\text{Turbulent: } C_f = \frac{0.455}{\{\log_{10} [\min(Re, Re_{cutoff})]\}^{2.58} (1 + 0.144 M^2)^{0.65}} \quad (3.14)$$

where  $Re$  is the Reynolds number over the characteristic length of the object ( $l$ ), that is the mean chord length for the wings and the entire length of the component for the fuselage and nacelles. In a turbulent flow over relatively rough surfaces, the value of  $C_f$  actually becomes higher than what the Eq. 3.14 using  $Re$  would result in. Therefore, a variable for cut-off Reynolds number ( $Re_{cutoff}$ ) was introduced to the model, and in Eq. 3.14 the minimum of the two Reynolds numbers is used. The value of  $Re_{cutoff}$  depends on  $l$  and the surface skin-roughness value ( $k$ ) and is determined by either of the two equations depending on the flow regime: [5]

$$Re_{cutoff} = \begin{cases} 38.21 \left(\frac{l}{k}\right)^{1.053} & M \leq 0.72 \text{ (subsonic)} \\ 44.62 \left(\frac{l}{k}\right)^{1.053} M^{1.16} & M > 0.72 \text{ (transsonic)} \end{cases} \quad (3.15)$$

Through the use of Eq. 3.14, the air compressibility effects are also taken into account in the drag estimation.

In order to determine the form factors for nacelles, their diameter ( $d_{nac}$ ) and length ( $l_{nac}$ ) values were estimated with empirical relations as a function of  $T_{static}$  of the engine [14]:

$$d_{nac} = 4 \left( 0.0625 + \frac{1}{4\sqrt{2}} \sqrt{1.730 \ln \frac{T_{static}}{1000} - \pi} \right) \quad (3.16)$$

$$l_{nac} = 5 \frac{\left(\frac{T_{static}}{1000}\right)^{0.9839}}{6 \pi \left(1.730 \ln \frac{T_{static}}{1000} - \pi\right)} \quad (3.17)$$

As the performance of turboprops is described by  $P_0$  rather than by  $T_{static}$ , a value for  $T_{static}$  to be used in Eqs. 3.16 and 3.17 was calculated with a relation presented by Sforza [15]:

$$T_{static} = \left( \frac{\pi}{2} \rho_0 d_{prop}^2 P_0^2 \right)^{1/3} \quad (3.18)$$

where  $d_{prop}$  is the propeller diameter that was introduced as a new user input parameter. The piston and electric engines were assumed to be installed completely inside the fuselage, and thus their contribution to the drag is here omitted. According to Isikveren [14], the Eqs. 3.16 and 3.17 are only valid for engines with  $T_{static} > 8.5$  kN. Nevertheless, the use of the equations was considered feasible here as turboprop, turbofan or turbojet engines with lower  $T_{static}$  are rare [11].

The form factors of the wings were estimated as a function of their thickness-to-chord ratios at mean chords  $(t/c)_{mean}$  [14]:

$$FF_w = 0.421 \left[ 2 + 4 \left( \frac{t}{c} \right)_{mean,w} + 240 \left( \frac{t}{c} \right)_{mean,w}^4 \right] \quad (3.19)$$

$$FF_{HT} = 1 + 0.1 \left( 1 - 0.893 \frac{|z_{HT,FRP}|}{h_{fus}} \right) \left[ 2 + 4 \left( \frac{t}{c} \right)_{mean,HT} + 240 \left( \frac{t}{c} \right)_{mean,HT}^4 \right] \quad (3.20)$$

$$FF_{VT} = 0.5 \left[ 2 + 4 \left( \frac{t}{c} \right)_{mean,VT} + 240 \left( \frac{t}{c} \right)_{mean,VT}^4 \right] \quad (3.21)$$

where  $z_{HT,FRP}$  is the z-coordinate of horizontal tail with respect to the fuselage reference plane, and  $h_{fus}$  is the maximum height of the fuselage. The  $(t/c)_{mean}$  values are functions of  $t$  and  $c$  at wing root and tip locations, all of which are user input parameters for all wings.

For fuselage and nacelles, the  $FF$  values were estimated as functions of their slenderness ratios [14]:

$$FF_{fus} = 1 + 0.0025 \left( \frac{l_{fus}}{h_{fus}} \right) + 60 \left( \frac{h_{fus}}{l_{fus}} \right)^3 \quad (3.22)$$

$$FF_{nac} = 1.17 \left[ 1 + 0.35 \left( \frac{d_{nac}}{l_{nac}} \right) \right] \quad (3.23)$$

where  $l_{fus}$  is the fuselage length, also an input parameter by the user.

According to Raymer [5], the interference factors for main wing and fuselage are negligible. Thus  $Q_w = Q_{fus} = 1$ . For nacelles,  $Q_{nac} = 1.3$  was used corresponding to an assumption of the engine installation distance being less than  $d_{nac}$  from wings or fuselage. For both tail wings, an interference factor of conventional tail was chosen, and thus  $Q_{HT} = Q_{VT} = 1.04$ .

The final factor to establish the  $C_{D,0,c}$  estimates through the component buildup method is the wetted area. For fuselage, the  $S_{\text{wet}}$  value was estimated through a relation presented by Torenbeek [4]:

$$S_{\text{wet,fus}} = C_{\text{fus}} l_{\text{fus}} \left(1 - \frac{2C_{\text{fus}}}{l_{\text{fus}}}\right)^{2/3} \left(1 + \frac{C_{\text{fus}}}{l_{\text{fus}}}\right)^2 \quad (3.24)$$

where  $C_{\text{fus}}$  is the maximum fuselage circumference, that is solved from the user input parameters for  $h_{\text{fus}}$  and fuselage maximum width ( $w_{\text{fus}}$ ). For the main wing, the estimate on  $S_{\text{wet}}$  by Torenbeek [4] was used:

$$S_{\text{wet,w}} = S_{\text{exp,w}} \left[1 + 0.25 \left(\frac{t}{c}\right)_{\text{root,w}} \frac{1 + \tau_w \lambda_w}{1 + \lambda_w}\right] \quad (3.25)$$

where  $\lambda$  is the wing taper ratio and  $\tau = (t/c)_{\text{tip}} / (t/c)_{\text{root}}$ . The exposed wing area ( $S_{\text{exp,w}}$ ) was estimated as double the  $S_{\text{ref,w}}$  minus the estimated square area that is inside the fuselage:

$$S_{\text{exp,w}} = 2(S_{\text{ref,w}} - c_{\text{root,w}} w_{\text{fus}}) \quad (3.26)$$

For  $S_{\text{wet,HT}}$ , the Eqs. 3.25 and 3.26 with corresponding horizontal tail values and by replacing  $w_{\text{fus}}$  with a user input parameter for fuselage width at horizontal tail quarter chord ( $w_{\text{fus,HT}}$ ) were used. Similarly, for  $S_{\text{wet,VT}}$  the Eq 3.25 with corresponding vertical tail values was used, and the exposed area was estimated as  $S_{\text{exp,VT}} = 2 S_{\text{ref,VT}}$ . Lastly, the empirical relation by Isikveren [14] for estimating  $S_{\text{wet,nac}}$  was used:

$$S_{\text{wet,nac}} = 0.4056 \pi^2 d_{\text{nac}} \left( \sqrt{0.2057 l_{\text{nac}}^2 + 0.04661 d_{\text{nac}}^2} + \sqrt{0.1853 l_{\text{nac}}^2 + 0.07557 d_{\text{nac}}^2} \right. \\ \left. - \sqrt{0.005077 l_{\text{nac}}^2 + 0.01611 d_{\text{nac}}^2} - \sqrt{0.01651 l_{\text{nac}}^2 + 0.03666 d_{\text{nac}}^2} \right) \quad (3.27)$$

The effect of an increase in angle of attack ( $\alpha$ ) to the drag of the wings was considered with the already modelled lift-induced drag and the stall behaviour, further described in Sec. 3.3.3. The effect of increasing  $\alpha$  to the drag of the nacelles is not considered. For fuselage, a simplified model of the effect of  $\alpha$  to its drag was implemented. The model consists of a function for the  $C_{D,\text{fus}}$  that follows a sinusoidal curve from  $C_{D,0,\text{fus}}$  at  $\alpha = 0$  to  $C_{D,\text{max,fus}}$  at  $\alpha = 90^\circ$  and  $\alpha = -90^\circ$ :

$$C_{D,\text{fus}} = \frac{C_{D,0,\text{fus}} - C_{D,\text{max,fus}}}{2} \cos(2\alpha) + \frac{C_{D,0,\text{fus}} + C_{D,\text{max,fus}}}{2} \quad (3.28)$$

where

$$C_{D,\text{max,fus}} = \frac{0.8 l_{\text{fus}} h_{\text{fus}}}{S_{\text{ref,w}}} \quad (3.29)$$

The  $C_{D,\text{max,fus}}$  corresponds to the drag coefficient of a cylinder perpendicular to the wind. The relation for  $C_{D,\text{max,fus}}$  given in [16] for the Reynolds numbers of around  $10^7$  to  $10^8$ , which are corresponding to the fuselage Reynolds numbers in flight, is normalised here with  $S_{\text{ref,w}}$  instead of the longitudinal cross section of the fuselage.

### 3.3.2 Lift

The lift curve slope of the main wing ( $C_{L_{\alpha,w}}$ ) was estimated as a function of the lift curve slope of its 2D airfoil ( $C_{l_{\alpha,w}}$ ) and other wing parameters and variables such that the air compressibility effects are also considered [5]:

$$C_{L_{\alpha,w}} = \frac{2 \pi AR_w}{2 + \sqrt{4 + \frac{AR_w^2 \beta^2}{\eta_w^2} \left(1 + \frac{\tan^2 \Lambda_w}{\beta^2}\right)}} \left( \frac{S_{\text{exp},w}}{2 S_{\text{ref},w}} \right) \left[ 1.07 \left(1 + \frac{w_{\text{fus}}}{b_w}\right)^2 \right] \quad (3.30)$$

where

$$\beta^2 = 1 - M^2 \quad (3.31)$$

$$\eta_w = \frac{C_{l_{\alpha,w}}}{2 \pi / \beta} \quad (3.32)$$

and  $AR$  is wing aspect ratio,  $\Lambda$  is wing sweep angle at quarter chord and  $b$  is wing span, the latter two of which are user input parameters.

Equation 3.30 was also used for  $C_{L_{\alpha,HT}}$  with the corresponding horizontal tail values and by replacing  $w_{\text{fus}}$  with  $w_{\text{fus,HT}}$  for  $C_{L_{\alpha,HT}}$ . As the vertical tail can be considered fully exposed, and there is no contribution to  $C_{L_{\alpha,VT}}$  by the fuselage due to the vertical tail spanning only to one side of the fuselage, the terms following the first fraction in Eq. 3.30 can be omitted for calculating the value for  $C_{L_{\alpha,VT}}$  resulting in

$$C_{L_{\alpha,VT}} = \frac{2 \pi AR_{VT}}{2 + \sqrt{4 + \frac{AR_{VT}^2 \beta^2}{\eta_{VT}^2} \left(1 + \frac{\tan^2 \Lambda_{VT}}{\beta^2}\right)}} \quad (3.33)$$

The contribution of the fuselage to the lift on its own was not estimated on any dedicated method for fuselage but through an empirical relation between the lift curve slopes of the wing-body combination ( $C_{L_{\alpha,wb}}$ ) and  $C_{L_{\alpha,w}}$  [14]:

$$C_{L_{\alpha,wb}} = C_{L_{\alpha,w}} \left[ \left(1 + 3.2 \frac{w_{\text{fus}}}{b_w}\right) \frac{S_{\text{exp},w}}{2 S_{\text{ref},w}} + \frac{\pi}{2 C_{L_{\alpha,w}}} \frac{w_{\text{fus}}^2}{S_{\text{ref},w}} \right] \quad (3.34)$$

The lift coefficient of the wing-body combination ( $C_{L,wb}$ ) before stall was then solved by assuming the lift curve slope of the fuselage to be  $C_{L_{\alpha,wb}}$  subtracted by  $C_{L_{\alpha,w}}$ :

$$C_{L,wb} = C_{L_{\alpha,w}} \alpha_{\text{eff},w} + (C_{L_{\alpha,wb}} - C_{L_{\alpha,w}}) \alpha \quad (3.35)$$

where  $\alpha_{\text{eff},w}$  is the effective angle of attack of the wing with the contribution of wing incidence  $i_w$ , wing zero-lift angle of attack and induced angle of attack due to wing dihedral in sideslip. The derivation for  $C_{L_{\alpha,wb}}$  was necessary not only for the fuselage contribution to the lift force but also for solving the stability derivative coefficient for change in roll moment due to roll rate ( $C_{l_p}$ ) and the control derivative coefficient for change in roll moment due to aileron deflection ( $C_{l_{\delta_a}}$ ) as it is a factor in their definitions.

### 3.3.3 Stall Behaviour

The stall behaviour for the main wing and horizontal tail was solved as a parametric analytical geometry problem where a combination of parabolic curves are generated as a function of  $C_{L_{\alpha}}$  and the maximum lift coefficient for the wing ( $C_{L_{\text{max}}}$ ). The value for  $C_{L_{\text{max}}}$  was solved by a relation presented by Raymer [5]

$$C_{L_{\text{max}}} = 0.9 C_{l_{\text{max}}} \cos \Lambda \quad (3.36)$$

where  $C_{l_{\max}}$  is the user input parameter for maximum lift coefficient of the 2D airfoil. The parabolic curves were solved such that they would mimic the  $C_L$  curves over  $\alpha$  right before and long after the point where  $C_{L_{\max}}$  is achieved. References [17] and [18] were studied for before and after stall behaviour of  $C_L$  values. The following conclusion from post stall studies were made, that would together with a requirement of differentiable function fully define a set of three second order functions:

1. The parabola around  $C_{L_{\max}}$  is 8 degrees wide.
2. At  $\alpha_{\text{eff}} = \alpha_{\text{eff}, C_L = C_{L_{\max}}} + \frac{1}{4} (90^\circ - \alpha_{\text{eff}, C_L = C_{L_{\max}}})$  the derivative  $\frac{\partial C_L}{\partial \alpha} = 0$ .
3. At  $\alpha_{\text{eff}} = 90^\circ$ , the  $C_L = 0$ .

By using the  $\alpha_{\text{eff}}$ , in the linear part of the  $C_L$  vs.  $\alpha$  curve, i.e. when  $\frac{\partial C_L}{\partial \alpha} = C_{L_\alpha}$ , the  $C_L$  is by definition 0 at  $\alpha_{\text{eff}} = 0$  for the main wing and horizontal tail. For  $\alpha_{\text{eff,HT}}$ , also the downwash angle ( $\epsilon$ ) generated by the main wing and the induced angle of attack for horizontal tail due to pitching rate ( $q$ ) are considered. The definition for the parabolic curves after the linear part are also graphically shown in Fig. 3.2, where the different linear and parabolic curves of the functions are shown in different colours.

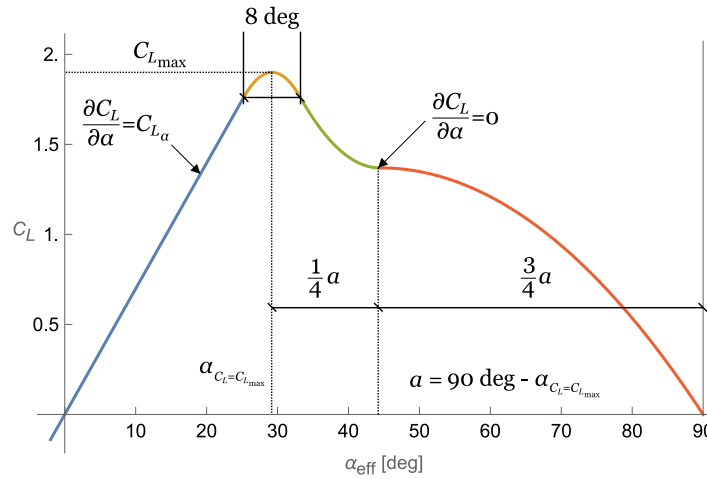


**Figure 3.2:**  $C_L$  vs.  $\alpha$  curves showing the constraints defining the second order functions to model stall in the library.

The results of the post stall studies showed however that the shape of the  $C_L$  vs.  $\alpha$  curve after stall varies with  $AR$  and  $\lambda$ . The practiced method here was still deemed adequate for predicting stall behaviour in conceptual design stage.

A study on the  $C_D$  vs.  $\alpha$  during stall was also conducted, and based on its findings the following assumptions for modelling the post stall  $C_D$  vs.  $\alpha$  curve were made:

1. The  $C_D$  of a wing stops following the  $C_{D,0} + C_{D,i}$  curve when  $\alpha_{\text{eff}} > \alpha_{\text{eff}, C_L = C_{L_{\max}}}$  [19]
2. When  $\alpha_{\text{eff}} > \alpha_{\text{eff}, C_L = C_{L_{\max}}}$ , the curve starts following a sinus curve until  $C_{D_{\max}}$  is achieved at  $\alpha_{\text{eff}} = 90^\circ$  [20].

Here the requirement for a continuous function was kept but the requirement for a differentiable function was rejected as the  $C_D$  vs.  $\alpha$  slope experienced an abrupt increase at  $\alpha_{\text{eff}, C_L = C_{L_{\max}}}$  also in the studied stall experiments. The  $C_{D_{\max}}$  was calculated with a formula for  $C_D$  of a flat plate perpendicular to the wind as a function of its  $AR$  [21]:

$$C_{D_{\max}} = 1.98 - 0.81 \left[ 1 - e^{\left(-\frac{20}{AR}\right)} \right] \quad (3.37)$$

Fig. 3.3 shows graphically the definition and the required parameters for the sinus curve to model post stall  $C_D$ .  $K$  is the induced drag factor for a wing, and its definition was already implemented in the Aircraft Library.

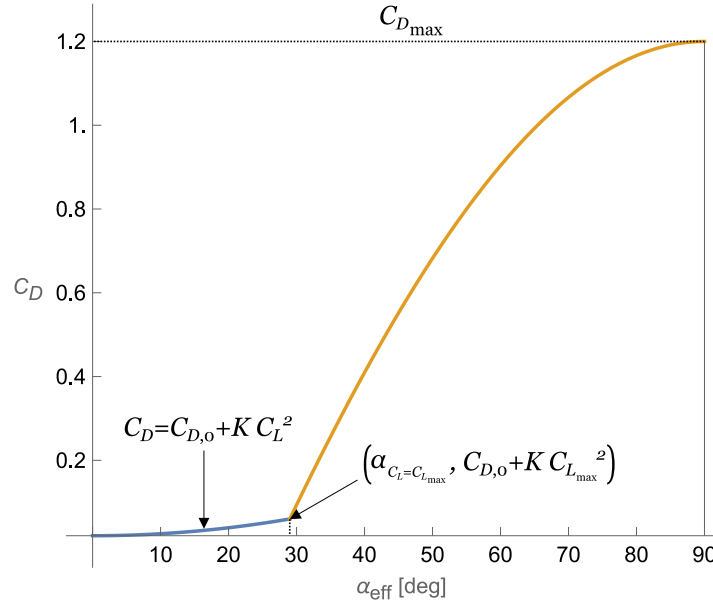


**Figure 3.3:** Definitions for a sinus function to model  $C_D$  vs.  $\alpha$  with an example showing the curve for wing with  $C_{D_{\max}} = 1.2$ .

### 3.3.4 Other Aerodynamic Coefficients

In addition to the lift and drag coefficients, there were two aerodynamic coefficients left as a user input parameter that were to be estimated based on the aircraft geometry, namely the sidewash due sideslip angle ( $\frac{\partial \sigma}{\partial \beta}$ ) and the empirical factor for estimating yaw due to aileron deflection control derivative coefficient ( $K_{C_{n_{\delta_a}}}$ ).

For estimating the value for  $\frac{\partial \sigma}{\partial \beta}$ , the an empirical relation presented in USAF DATCOM [22] was used:

$$\frac{\partial \sigma}{\partial \beta} = -0.276 + 3.06 \frac{\frac{S_{\text{ref,VT}}}{S_{\text{ref,w}}}}{1 + \cos \Lambda_w} + 0.4 \frac{\left( -\tan \Gamma_w \frac{y_{w,AC} - w_{\text{fus}}}{2} \right) + z_{w,\text{root}}}{w_{\text{fus}}} + 0.009 AR_w \quad (3.38)$$

where  $\Gamma_w$  is the main wing dihedral angle,  $y_{w,AC}$  is the y-coordinate of main wing aerodynamic centre with respect to fuselage centreline and  $z_{w,\text{root}}$  is the z-coordinate of main wing root with respect to the fuselage reference plane.

The value of  $K_{C_{n_{\delta_a}}}$  is a function of  $AR_w$ ,  $b_w$  and the y-coordinate of the inboard edge of the aileron ( $y_{a,\text{root}}$ ). Its value was previously left for the user to determine from the dedicated curve chart found in reference [10]. The numerical data from the curve chart was extracted into a table, and a function of  $AR$ ,  $b_w$  and  $y_{a,\text{root}}$  was fitted on the table data resulting in an equation for estimating  $K_{C_{n_{\delta_a}}}$ :

$$K_{C_{n_{\delta_a}}} = -0.350894 - 0.066355 \left( \frac{2 y_{a,\text{root}}}{b_w} \right)^{4.15179} + 0.029308 AR_w \quad (3.39)$$

and the chart is replicated here using Eq. 3.39 in Fig. 3.4.

$$\eta = \frac{2 y_{a, \text{root}}}{b_w}$$

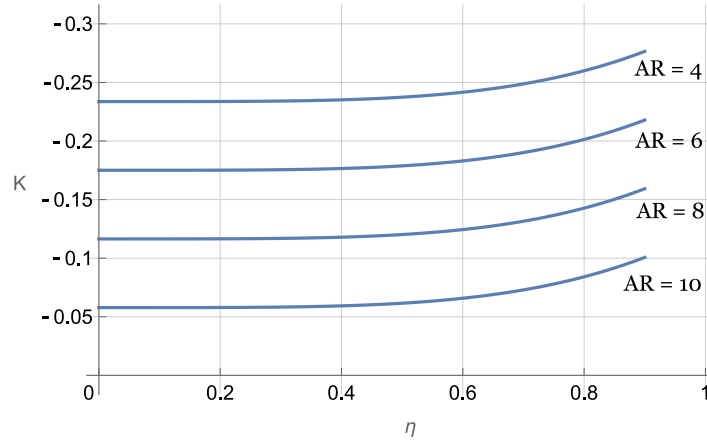


Figure 3.4: Curve chart for estimating  $K_{C_{n_{\delta_a}}}$ .

### 3.4 Weight Estimation

The library previously required the entire weight of the aircraft, its CG location and inertia tensor as an input parameter by the user. This was to be developed such that the all mass properties are estimated based on the geometrical input parameters and some design variables while also keeping the option to input the mass properties directly to the library should they be known or estimated outside the library. For this purpose, a new boolean input parameter was introduced to switch between these options.

To estimate the weight of fuselage, main wing, horizontal and vertical tail, the empirical weight estimation methods by Nicolai [23] were used. The method presents two relations for each component, one for light utility aircraft and one for larger aircraft. The limit between the two groups was set to a design cruise Mach number ( $M_{\text{des}}$ ) of 0.4. The weight estimation method required also additional design parameters, that are design maximum take-off mass ( $m_{\text{MTO,des}}$ ), maximum dynamic pressure ( $q_{\text{max}}$ ) and maximum load factor ( $n_{\text{max}}$ ), which were introduced as new user input parameters to the model. For other components, other statistical relation from various sources were used, and they are presented in their respective sections.

#### 3.4.1 Fuselage

The equations given in Nicolai [23] are all to be used with imperial units but here they are converted to work with SI-units. The equations for the weight of the fuselage ( $m_{\text{fus}}$ ) are functions of the new design parameters and the fuselage dimensions:

$$m_{\text{fus}} = \begin{cases} 0.0837767 [l_{\text{fus}}^{0.857} (h_{\text{fus}} + w_{\text{fus}}) (m_{\text{MTO,des}} n_{\text{max}})^{0.286} v_{\text{max},0}^{0.338}]^{1.1} & M_{\text{des}} \leq 0.4 \\ 0.001287 m_{\text{MTO,des}}^{0.95} q_{\text{max}}^{0.283} \left( \frac{l_{\text{fus}}}{h_{\text{fus}}} \right)^{0.71} & M_{\text{des}} > 0.4 \end{cases} \quad (3.40)$$

where  $v_{\text{max},0}$  is the maximum airspeed at sea level and is calculated here as a function of the new  $q_{\text{max}}$  input parameter:

$$v_{\text{max}} = \sqrt{\frac{2 q_{\text{max}}}{\rho_0}} \quad (3.41)$$

Only the fuselage structural weight, excluding the weight of payload and all systems onboard, is included in  $m_{fus}$ . If advanced composite materials are used, that is indicated by a dedicated boolean user input parameter, then a factor of 0.75 is added into Eq. 3.40 to represent the consequent weight reduction [23].

### 3.4.2 Main Wing

Similarly, the equations to estimate the weight of the main wing ( $m_w$ ) are functions of the new design parameters and wing geometric parameters [23]:

$$m_w = \begin{cases} 0.011409 \left\{ S_{ref,w}^{0.61} (m_{MTO,des} n_{max})^{0.65} (1 + 0.0038876 v_{max})^{0.5} \right. \\ \quad \left. \times \left( AR_w \frac{1}{\cos \Lambda_w} \right)^{0.57} \left[ \frac{c_{root,w}(1 + \lambda_w)}{t_{root,w}} \right]^{0.36} \right\}^{0.993} & M_{des} \leq 0.4 \\ \frac{5.00928 AR_w S_{ref,w}^{0.48} \lambda_w^{0.14} (m_{MTO,des} n_{max})^{0.84} M_{max,0}^{0.43}}{10^4 \left( \frac{t_{root,w}}{c_{root,w}} \right)^{0.76} \cos \Lambda_{w,HC}^{1.54}} & M_{des} > 0.4 \end{cases} \quad (3.42)$$

where  $M_{max,0}$  is the maximum Mach number at sea level, that is  $v_{max,0}$  divided by speed of sound at sea level ( $a_0$ ), and  $\Lambda_{w,HC}$  is the main wing sweep angle at half chord. The value for  $\Lambda_{w,HC}$  is calculated from  $\Lambda_w$  and the wing dimensions:

$$\Lambda_{w,HC} = \tan^{-1} \left( \frac{2 b_w \tan \Lambda_w - c_{root,w} + c_{tip,w}}{2 b_w} \right) \quad (3.43)$$

If advanced composite materials are used, the factor added to Eq. 3.42 is 0.8 [23].

### 3.4.3 Tail

The equations for horizontal tail weight estimation ( $m_{HT}$ ) are functions of horizontal tail geometry, its position,  $m_{MTO,des}$  and  $n_{max}$  [23]:

$$m_{HT} = \begin{cases} 0.122722 \left[ l_{HT}^{0.483} S_{ref,HT}^{1.2} \left( \frac{b_{HT}}{t_{root,HT}} \right)^{0.5} (m_{MTO,des} n_{max})^{0.87} \right]^{0.458} & M_{des} \leq 0.4 \\ 0.0133656 \left[ S_{ref,HT}^{0.584} \left( \frac{b_{HT}}{t_{root,HT}} \right)^{0.033} \left( \frac{c_{mean,HT}}{l_{HT}} \right)^{0.28} \right. \\ \quad \left. \times (m_{MTO,des} n_{max})^{0.813} \right]^{0.915} & M_{des} > 0.4 \end{cases} \quad (3.44)$$

where  $l_{HT}$  is the horizontal tail lever arm measured from main wing aerodynamic centre to horizontal tail mean quarter chord. The horizontal tail mean chord was solved through the equation for mean chord of an arbitrary tapered wing [24]:

$$c_{mean,HT} = \frac{2}{3} c_{root,HT} \frac{1 + \lambda_{HT} + (\lambda_{HT})^2}{1 + \lambda_{HT}} \quad (3.45)$$

Similarly to horizontal tail, the weight of vertical tail ( $m_{VT}$ ) is estimated as a function of its geometry, position and the design parameters [23]:

$$m_{VT} = \begin{cases} 0.000112407 S_{ref,VT}^{1.2} \left( \frac{b_{VT}}{t_{root,VT}} \right)^{0.5} (m_{MTO,des} n_{max})^{0.87} & M_{des} \leq 0.4 \\ 0.769664 \left\{ AR_{VT}^{0.337} S_{ref,VT}^{1.089} [(1 + \lambda_{VT}) m_{MTO,des} n_{max}]^{0.363} \right. \\ \times \left( 1 + \frac{S_r}{S_{ref,VT}} \right)^{0.217} M_{max,0}^{0.601} l_{VT}^{-0.726} \cos \Lambda_{VT}^{-0.484} & M_{des} > 0.4 \\ \times \left[ 1 - \frac{\min(0, z_{HT,FRP} - z_{VT,root})}{b_{VT}} \right]^{0.5} \left. \right\}^{1.014} & \end{cases} \quad (3.46)$$

where  $S_r$  is the rudder area (on one side),  $z_{VT,root}$  is the z-coordinate of vertical tail root chord with respect to fuselage reference plane and  $l_{VT}$  is the vertical tail arm length measured from main wing aerodynamic centre to vertical tail aerodynamic centre. The reduction factor to be added to Eqs. 3.44 and 3.46 if advanced composite materials are used, is 0.75 [23].

For the lever arm values, aerodynamic centre locations of horizontal and vertical tail were first solved with the help of equations given in reference [24]. Thus, the values for  $l_{HT}$  and  $l_{VT}$  were able to be solved with the existing user input parameters:

$$l_{HT} = |x_{HT,root,LE}| + \tan \Lambda_{HT,LE} \frac{b_{HT} - w_{fus,HT}}{2} \frac{1 + 2 \lambda_{HT}}{3 + 3 \lambda_{HT}} + \frac{c_{mean,HT}}{4} - |x_{w,AC}| \quad (3.47)$$

$$l_{VT} = |x_{VT,root,LE}| + \tan \Lambda_{VT,LE} b_{VT} \frac{1 + 2 \lambda_{VT}}{3 + 3 \lambda_{VT}} + \frac{c_{mean,VT}}{4} - |x_{w,AC}| \quad (3.48)$$

where  $x_{HT,root,LE}$  and  $x_{VT,root,LE}$  are the x-coordinates of horizontal and vertical tail root chord leading edges measured from  $c_{mean,w}$  leading edge, and  $x_{w,AC}$  is the x-coordinate of main wing aerodynamic centre with respect to  $c_{mean,w}$  leading edge. The mean aerodynamic chord of vertical tail ( $c_{mean,VT}$ ) was calculated with Eq. 3.45 using corresponding vertical tail values. The sweep angles at horizontal and vertical tail leading edges were solved similarly to  $\Lambda_{w,HC}$  through trigonometry:

$$\Lambda_{HT,LE} = \tan^{-1} \left( \frac{c_{root,HT} - c_{tip,HT} + 2 b_{HT} \tan \Lambda_{HT}}{2 b_{HT}} \right) \quad (3.49)$$

$$\Lambda_{VT,LE} = \tan^{-1} \left( \frac{c_{root,VT} - c_{tip,VT} + 4 b_{VT} \tan \Lambda_{VT}}{4 b_{HT}} \right) \quad (3.50)$$

### 3.4.4 Engines

The weight estimation method by Isikveren [14] was used to estimate the weight of turboprop, turbofan and turbojet engines including installation. The method gives a statistical relation between the installed engine mass ( $m_{eng}$ ) and  $T_{static}$ . For turboprop, the relations reads as:

$$m_{eng} = 0.016316586 (T_{static})^{1.0572} + 0.00613 T_{static} \quad (3.51)$$

For turbofan and turbojet engines, the relation depends additionally on whether the engine has a thrust-reverser:

$$m_{eng} = \begin{cases} 0.0157365 T_{static}^{1.0572} + 0.02173185 T_{static}^{0.7780992} & \delta_{T,neg,max} = 0 \\ 0.01646307 T_{static}^{1.0572} + 0.02173185 T_{static}^{0.7780992} & \delta_{T,neg,max} > 0 \end{cases} \quad (3.52)$$

where  $\delta_{T,\text{neg,max}}$  is the user input parameter for maximum negative thrust of the engine as a fraction of  $T_{\text{avail}}$  (having the allowed range from 0 to 1). For turboprops, there is no weight addition from the existence of a thrust-reverser as for them the thrust reverser is usually deployed simply by changing the propeller blade pitch angle instead of redirecting the exhaust gas inside the nacelle [13].

For piston engines, the statistical relation between uninstalled engine weight and  $P_0$  presented by Gudmundsson [11] and the statistical relation between uninstalled and installed engine weight of a light utility aircraft by Nicolai [23] were combined to establish relation between installed engine weight and  $P_0$ :

$$m_{\text{eng}} = 0.0045394 (P_0 - 16076.3)^{0.922} \quad (3.53)$$

Well established statistical relation between aircraft electric engine weight and its  $P_0$  was not found, and thus the electrical engine weight was estimated with a conservative engine specific power value of 4,000 W/kg based on the data in references [25] and [26]. The rule of thumb for adding 25 % for electric engine installation by Nicolai [23] was used for solving the installed electric engine weight resulting in

$$m_{\text{eng}} = \frac{P_0}{3200} \quad (3.54)$$

### 3.4.5 Fuel Tanks

The volumes of the fuel tanks were estimated with existing methods and a new user input parameter was introduced for the fuel density to be used to calculate the fuel tank weight. The structural weight of all tanks was assumed to be included in fuselage and wing structural weights, and therefore the weight of the fuel tanks is purely the product of their volume and the given fuel density. New user input parameters were also introduced to reduce the fuel tank volumes with a fudge factor and to set a fraction of total tank volume to be used as an initial fuel volume for the flight mission. During the simulation, the fuel weight is retracted by the amount of burned fuel according to the calculations presented in Sec. 3.2.

For the centre fuel tank, the volume  $V_{\text{ctrf}}$  was estimated using a statistical relation presented by Ding and Zhang [27]:

$$V_{\text{ctrf}} = \frac{2111}{2750} c_{\text{root,w}} t_{\text{root,w}} w_{\text{fus}} \quad (3.55)$$

For estimating the volume of wing fuel tank volume on one side of the main wing ( $V_{\text{wf}}$ ), the Torenbeek method for a continuous wing fuel tank disregarding any breaks at the spanwise location of the engines was used [4]:

$$V_{\text{wf}} = 0.27 \frac{S_{\text{ref,w}}^2 t_{\text{root,w}} (1 + \lambda_w \sqrt{\tau_w} + \lambda_w^2 \tau_w)}{b_w c_{\text{root,w}} (1 + \lambda_w)^2} \quad (3.56)$$

### 3.4.6 Battery

For estimating the weight of the battery ( $m_{\text{batt}}$ ) for aircraft with electric propulsion, two new user input parameters were introduced for the specific energy ( $e_{\text{cell}}$ ) and energy density ( $U_{\text{cell}}$ ) of the battery cells. Additionally, the gross capacity of the battery system ( $E_{\text{batt}}$ ) was left for the user to input as a parameter. In order to add the weight due to casing, cooling and installation of the battery system, the statistical relations between the  $e$  and  $U$  values on battery cell and battery system levels for a battery consisting of cylindrical battery cells presented by L bberding et al. [28] were used:

$$e_{\text{batt}} = 2.613 e_{\text{cell}} - 0.14690 \quad (3.57)$$

$$U_{\text{batt}} = 0.847 U_{\text{cell}} - 1.05986 \times 10^{-4} \quad (3.58)$$

The equations above only work with standard SI-units for specific energy (J/kg) and energy density (J/m<sup>3</sup>). The given  $E_{\text{batt}}$  value by the user is divided by  $e_{\text{batt}}$  and  $U_{\text{batt}}$  to get the mass and volume of the battery system, respectively.

### 3.4.7 Landing Gear

For the landing gear, the weight estimation method presented by Isikveren [14] was used since it couples the  $m_{\text{MTO,des}}$  value with landing gear strut length, landing touch down speed and tyre inflation pressure, and thus no new user input parameters were required to be introduced for landing gear. The Isikveren method for the landing gear weight ( $m_{\text{lg}}$ ) is a function of  $m_{\text{MTO,des}}$  and the mounting of the main wing and engines:

$$m_{\text{lg}} = [587 - 153(\Phi_1 + \Phi_2)] \left( \frac{m_{\text{MTO,des}}}{1.4 \times 10^4} \right)^{1.05} \quad (3.59)$$

where

$$\Phi_1 = \begin{cases} 0 & \text{fuselage mounted engines} \\ 1 & \text{wing mounted engines} \end{cases} \quad (3.60)$$

$$\Phi_2 = \begin{cases} 0 & 0.5 - z_{\text{w,root}}/h_{\text{fus}} \leq 0.25 \\ 1 & 0.5 - z_{\text{w,root}}/h_{\text{fus}} > 0.25 \end{cases} \quad (3.61)$$

### 3.4.8 Systems

Instead of estimating the weight of each component of the systems installed onboard, the simple estimate for the entire systems weight ( $m_{\text{sys}}$ ) presented by Isikveren [14] was used:

$$m_{\text{sys}} = 0.6 k_{\text{pax}} n_{\text{pax}} \quad (3.62)$$

where  $n_{\text{pax}}$  is the design number of passengers, and  $k_{\text{pax}}$  is the constant weight passenger coefficient which Isikveren has derived from  $n_{\text{pax}}$  and the number of seats abreast ( $n_{\text{abs}}$ ):

$$k_{\text{pax}} = \begin{cases} 55.168 + 10.344 n_{\text{abs}} - 3.9865 n_{\text{pax}}^{0.3494} & n_{\text{pax}} \leq 180 \\ 69.12 + 12.96 n_{\text{abs}} - 3.9865 n_{\text{pax}}^{0.3494} & n_{\text{pax}} > 180 \end{cases} \quad (3.63)$$

The two equations for  $k_{\text{pax}}$  depending on the limit of  $n_{\text{pax}} = 180$  is based on the assumption by Isikveren that aircraft with more than 180 passengers have two aisles in the cabin. The value for  $n_{\text{abs}}$  was derived here from  $w_{\text{fus}}$  and a seat width of  $w_{\text{seat}} = 0.5588$  m, that represents the wide end of the seat widths in use in economy class [23]:

$$n_{\text{abs}} = \begin{cases} \left\lceil \frac{0.9 w_{\text{fus}}}{w_{\text{seat}}} \right\rceil & n_{\text{pax}} \leq 180 \\ \left\lceil \frac{0.9 w_{\text{fus}}}{w_{\text{seat}}} \right\rceil - 1 & n_{\text{pax}} > 180 \end{cases} \quad (3.64)$$

The used method for estimating systems weight is indeed best to be used for commercial passenger aircraft while giving more underestimated values of  $m_{\text{sys}}$  for smaller general aviation aircraft or cargo aircraft.

### 3.4.9 Payload

The weight of the payload ( $m_{PL}$ ) was left for the user to enter as its value is critical for the purpose of aircraft conceptual design and may vary greatly among different aircraft with otherwise similar design variables. The user is however advised to use standard passenger and baggage weights by FAA [29], shown in Tab. 3.1, to be multiplied by  $n_{pax}$  for passenger aircraft.

**Table 3.1:** Standard passenger and baggage weights. [29]

Season	Adult [kg]	Baggage [kg]
Summer	81.6	11.3* 13.6**
Winter	83.9	11.3* 13.6**

\* Domestic flight. \*\* International flight.

## 3.5 Centre of Gravity Location

In order to get a correct CG location for the entire aircraft, the CG locations within each component need to be determined along with the coordinates of each component with respect to a set reference point. The reference point in the model is set to a fuselage reference point that is half of all given maximum fuselage dimensions, shown in Fig. 3.5.

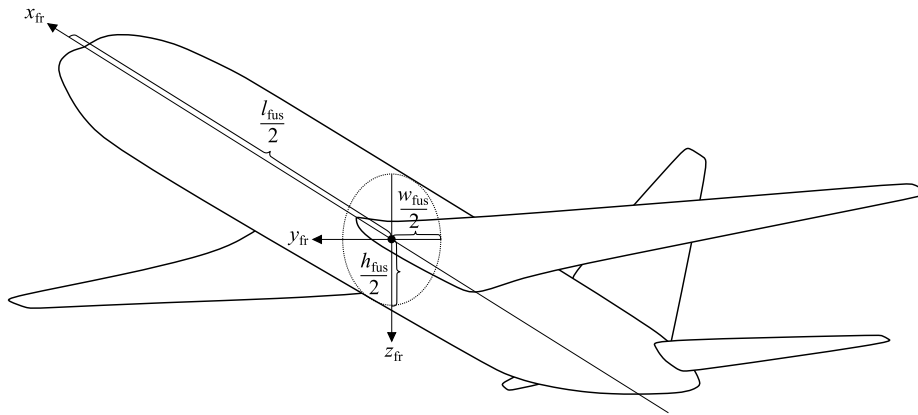


**Figure 3.5:** Reference point from which the coordinates of the origin of components are measured from.

### 3.5.1 Fuselage

According to Roskam [30], the CG location of the fuselage depends on the propulsion configuration. Table 3.2 shows how the data given in [30] was implemented here with the restrictions existing in the library, namely the assumption of turboprop, electric and piston engines being tractor engines (propeller at front).

**Table 3.2:** CG locations for fuselage.

Propulsion configuration	CG Location
Single Engine	33.5 % of $l_{fus}$ from nose
Turboprop, Electric or Piston Engines (wing mounted)	39.0 % of $l_{fus}$ from nose
Turbofan or Turbojet Engines (wing mounted)	43.5 % of $l_{fus}$ from nose
Any Engine (rear fuselage mounted)	48.5 % of $l_{fus}$ from nose

### 3 .5.2 Wings

Reference [30] was examined for determining the CG locations of each component. For wings, the CG locations were given as a fraction of the wing semispan and a fraction of the chord length at the given spanwise location, as shown in Tab. 3 .3.

Table 3 .3: CG locations for wings.

Component	Spanwise CG Location	Chordwise CG Location
Unswept Wing (half)	40 % of semispan	40 % of chord length from LE
Swept Wing (half)	35 % of semispan	50 % of chord length from LE
Horizontal Tail (half)	38 % of semispan	42 % of chord length from LE
Vertical Tail	38-55 %* of semispan	42 % of chord length from LE

\* Depending on horizontal tail z-coordinate. Equation shown in Appendix A .1.

However, when considering the contribution of the CG locations and inertia tensors of the wings to the CG location and inertia tensor of the entire aircraft, the  $\Gamma_w$ ,  $i_w$  and  $i_{HT}$  angles needed to be considered (dihedral angle for horizontal tail is not modelled), as a change in their value will shift the wing CG with respect to the fuselage reference point.

For the main wing, the CG location was solved on each side with respect to its root quarter chord in a frame where xy-plane is parallel to the wing surface such that the values given in reference [30] were convenient to use. Fixed rotation with a rotation sequence of first  $\Gamma_w$  ( $-\Gamma_w$  for left wing) around body x-axis and then  $i_w$  around the resulting y-axis was put after the fixed translation from the fuselage reference point to wing root quarter chord. Thus, a change in  $\Gamma_w$  and  $i_w$  results in a correct change in the half wing CG locations. However, this method also required all spanwise distances to be divided by  $\cos \Gamma_w$  as the wing span is measured on xy-plane on the body frame. The CG location on horizontal tail was solved on a frame rotated  $i_{HT}$  around the body y-axis.

The equations for solving all wing origin coordinates with respect to the fuselage reference point and the CG coordinates within the wings are found in Appendix A .1.

### 3 .5.3 Engines

The CGs of turboprop, turbofan and turbojet engines were estimated to be in their nacelle geometric centroids based on the calculated variables of  $l_{nac}$  and  $d_{nac}$ . For piston and electric engines, the CG is at the exact position according to the user input parameters stating the engine locations.

### 3 .5.4 Fuel Tanks

The CG location of the fuel tanks was solved individually for centre fuel tank and the tanks on each side of the main wing. The CG of the centre fuel tank is at half wing root chord on the body x-axis and at fuselage centreline on the body y-axis. The CG of the wing fuel tanks is at the geometric centroid of the tank trapezoid, which has its dimensions and position within the wings shown in Fig. 3 .6 together with the centre tank. The wing fuel tank trapezoid dimensions are based on the data given by Isikveren [14].

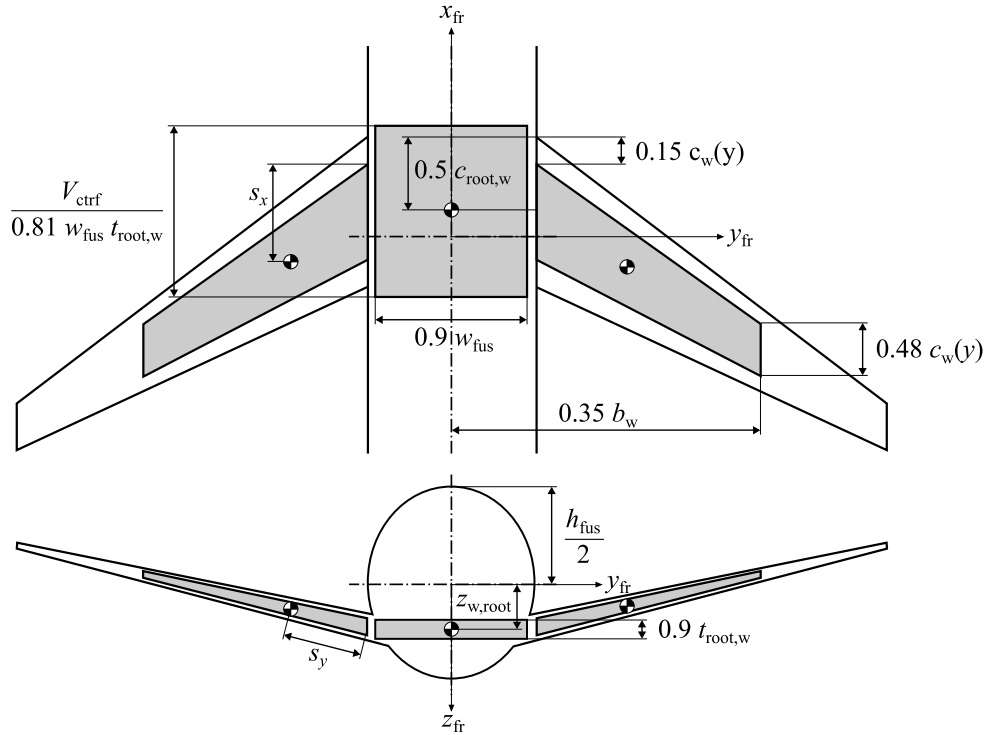


Figure 3.6: Dimensions and CG locations of the wing and centre tanks.

The wing fuel tank coordinates ( $s_x$  and  $s_y$ ) are the coordinates for the geometric centroid of an arbitrary trapezoid [31]:

$$s_x = \frac{2ac + a^2 + cb + ab + b^2}{3(a + b)} \quad (3.65)$$

$$s_y = \frac{h}{3} \left( \frac{2a + b}{a + b} \right) \quad (3.66)$$

where

$$h = \frac{0.7 b_w - w_{fus}}{2 \cos \Gamma_w} \quad (3.67)$$

$$a = c_{root,w} + \frac{0.96 h(c_{tip,w} - c_{root,w})}{b_w - w_{fus}} \quad (3.68)$$

$$b = 0.48 c_{root,w} \quad (3.69)$$

$$c = \frac{0.3 h(c_{tip,w} - c_{root,w})}{b_w - w_{fus}} + h \tan \Lambda_{w,LE} \quad (3.70)$$

The sweep angle at the main wing leading edge was solved with the sweep angle at quarter chord and the wing dimensions:

$$\Lambda_{w,LE} = \tan^{-1} \left( \frac{2 b_w \tan \Lambda_w - c_{tip,w} + c_{root,w}}{2 b_w} \right) \quad (3.71)$$

Figure 3.6 shows that setting the wing fuel tank CG to the geometric centroid of the 2D trapezoid is not completely accurate as the change in the thickness of the tank along the semispan is thus disregarded which, had it been implemented, would have resulted in a more inboard CG location. However, the implemented simplified wing fuel tank model

also disregards the cut in the tank that exists at the spanwise location of wing mounted engines [14], which on the other hand would shift the CG outboard. Hence, the implemented simplification of the fuel wing tank was considered adequate although the inaccuracy still remains with fuselage mounted engines. The CG locations of the fuel tanks were considered fixed over time despite the burning of the fuel.

### 3.5.5 Battery

For aircraft with electric propulsion, the battery system CG location has a large impact on the aircraft longitudinal stability and it is essential to be able to shift it with ease during the aircraft conceptual design process. Thus, the battery system CG location on body x-axis was left for the user to decide directly through a new input parameter. On body y-axis the CG location was assumed to be at the fuselage centreline. Due to the modelled shape of the battery system described in Sec. 3.6, its CG location on body z-axis resulted in  $0.159075 h_{\text{fus}}$  below the fuselage reference plane.

### 3.5.6 Landing Gear

When it comes to the landing gear, there usually are two different configurations in use, namely the tricycle and taildragger landing gears. The rule to position the landing gear correctly includes that for tricycle landing gear the heavier main landing gear is slightly aft of the aircraft CG while the lighter nose gear sits far in the front. For taildragger landing gear it is the opposite, and thus an assumption was made to locate the landing gear CG always at the guessed aircraft CG along the body x-axis. For this purpose, a guessed value of 15 % of  $c_{\text{mean,w}}$  for the aircraft CG was used. In body z-axis the landing gear CG was set to  $h_{\text{fus}}/2$  below the fuselage reference plane. [11]

### 3.5.7 Systems and Payload

The CG location for all the systems installed onboard is the same as fuselage CG as the moment of inertia estimation method used for fuselage takes also the weight distribution of the systems into account. For payload, the fuselage reference point shown in Fig. 3.5 was used as its CG location.

## 3.6 Inertia Tensor

The moment of inertia estimation methods given in USAF DATCOM [22] were used to determine the moments of inertia for main wing, horizontal tail, vertical tail and fuselage (with systems installed onboard). The final form of the implemented equations in the model are shown in detail in Appendix A.2. For other components, the moment of inertia equations for simple solid 3D shapes were used.

### 3.6.1 Engines

The moments of inertia for turboprop, turbofan and turbojet engines were estimated as them being solid cylinders:

$$I_{xx,\text{eng}} = \frac{1}{2} m_{\text{eng}} \left( \frac{d_{\text{nac}}}{2} \right)^2 \quad (3.72)$$

$$I_{yy,\text{eng}} = I_{zz,\text{eng}} = \frac{1}{12} m_{\text{eng}} \left[ 3 \left( \frac{d_{\text{nac}}}{2} \right)^2 + l_{\text{nac}}^2 \right] \quad (3.73)$$

The piston and electric engines were considered as point masses without moments of inertia.

### 3.6.2 Fuel Tanks

The centre fuel tank was also considered as a box. The width of the centre tank was set to 90 % of  $w_{fus}$ , and the height of the tank was set to 90 % of  $t_{root,w}$ . Thus, by knowing the two dimensions and the volume of the centre fuel tank, its moments of inertia could be solved similarly to the moments of inertia of the payload:

$$I_{xx,ctrf} = \frac{1}{12} m_{ctrf} [(0.9 w_{fus})^2 + (0.9 t_{root,w})^2] \quad (3.74)$$

$$I_{yy,ctrf} = \frac{1}{12} m_{ctrf} \left[ \left( \frac{V_{ctrf}}{0.81 w_{fus} t_{root,w}} \right)^2 + (0.9 t_{root,w})^2 \right] \quad (3.75)$$

$$I_{zz,ctrf} = \frac{1}{12} m_{ctrf} \left[ \left( \frac{V_{ctrf}}{0.81 w_{fus} t_{root,w}} \right)^2 + (0.9 w_{fus})^2 \right] \quad (3.76)$$

The moments of inertia for wing fuel tanks were estimated with the equations for radius of gyration ( $r_g$ ) of an arbitrary 2D trapezoid and the relation between moment of inertia and radius of gyration around an axis:

$$I = m r_g^2 \quad (3.77)$$

The  $r_g$  around different axes was calculated with the equations given in reference [31], and together with Eq. 3.77 the moments of inertia for one trapezoidal wing fuel tank ( $I_{wf}$ ) were calculated as functions of the tank dimensions on a frame that is parallel to the wing surface, as was done to the main half wing CG location:

$$I_{xx,wf} = m_{wf} \frac{h^2}{36} \left[ 2 + \frac{4ab}{(a+b)^2} \right] \quad (3.78)$$

$$I_{yy,wf} = m_{wf} \frac{a^4 + 2a^3b + a^3c + a^2b^2 + 3a^2bc + 2ab^3 - 3ab^2c + 4abc^2 + b^4 - b^3c + b^2c^2}{18(a+b)^2} \quad (3.79)$$

$$I_{zz,wf} = I_{xx,wf} + I_{yy,wf} \quad (3.80)$$

where  $h$ ,  $a$ ,  $b$  and  $c$  are given by Eqs. 3.67, 3.68, 3.69 and 3.70, respectively. Using only the  $r_g$  values of a 2D trapezoid for solving the moments of inertia of the wing fuel tanks comes with the same inaccuracies discussed in Sec. 3.5 due to neglecting the thickening of the tank from tip to root.

As the weight of the tanks and consequently their moments of inertia are not constant, the Modelica Standard Library model for 6DOF body could not be used due to its limitation of accepting constant mass properties only. Instead, the gravitational force and the forces resisting linear and angular accelerations were solved and applied with force and torque components acting on the tank CG such that  $\sum \mathbf{F} = m\mathbf{a}$  and  $\boldsymbol{\tau} = \mathbf{I}\boldsymbol{\alpha}$ .

### 3.6.3 Battery

For aircraft with electric propulsion, the battery system was modelled as a solid box with a width of  $0.6363 w_{fus}$  and a height of  $0.31815 h_{fus}$ . The width of the box correspond to 90 % of the width for the largest possible rectangle fitted inside an ellipse [32]. Its height on the other hand is half of the 90 % of the corresponding rectangle height, and the top surface of the box was set on the fuselage reference plane. As the volume of the battery system was known, the length of the battery system box was also known, and the moments of inertia of the battery system could be solved with moment of inertia equations for a solid box:

$$I_{xx,\text{batt}} = \frac{1}{12} m_{\text{batt}} [(0.6363 w_{\text{fus}})^2 + (0.31815 h_{\text{fus}})^2] \quad (3.81)$$

$$I_{yy,\text{batt}} = \frac{1}{12} m_{\text{batt}} \left[ \left( \frac{V_{\text{batt}}}{0.202438845 w_{\text{fus}} h_{\text{fus}}} \right)^2 + (0.31815 h_{\text{fus}})^2 \right] \quad (3.82)$$

$$I_{zz,\text{batt}} = \frac{1}{12} m_{\text{batt}} \left[ \left( \frac{V_{\text{batt}}}{0.202438845 w_{\text{fus}} h_{\text{fus}}} \right)^2 + (0.6363 w_{\text{fus}})^2 \right] \quad (3.83)$$

### 3.6.4 Landing Gear

Within the range of the aircraft that can be modelled with the library, there is no standard shape for landing gears, and consequently a compromise was made to consider them as point loads without moments of inertia.

### 3.6.5 Payload

For the payload, the moments of inertia were estimated as it being a box inside the fuselage. The dimensions of the box were determined as  $0.8 l_{\text{fus}}$  along body x-axis,  $0.6363 w_{\text{fus}}$  along body y-axis and  $0.6363 h_{\text{fus}}$  along body z-axis. Similarly to the dimensions of the battery, the set value for payload width and height correspond to 90 % of the width and height of the largest possible rectangle fitted inside an ellipse. Thus, the equations of moments of inertia for a solid box were used with the corresponding box dimensions:

$$I_{xx,\text{PL}} = \frac{1}{12} m_{\text{PL}} [(0.6363 w_{\text{fus}})^2 + (0.6363 h_{\text{fus}})^2] \quad (3.84)$$

$$I_{yy,\text{PL}} = \frac{1}{12} m_{\text{PL}} [(0.8 l_{\text{fus}})^2 + (0.6363 h_{\text{fus}})^2] \quad (3.85)$$

$$I_{zz,\text{PL}} = \frac{1}{12} m_{\text{PL}} [(0.8 l_{\text{fus}})^2 + (0.6363 w_{\text{fus}})^2] \quad (3.86)$$

### 3.6.6 Products of Inertia

The products of inertia ( $I_{xy}$ ,  $I_{xz}$  and  $I_{yz}$ ) were not considered on the component level. However, as moments of inertia of each component are summed with their eventual lever arms with respect to the eventual CG of the entire aircraft, the products of inertia values for the entire aircraft emerge when the model is compiled for simulation, and they will contribute to the flight mechanics.

### 3.7 The Use of the Model in Aircraft Sizing

Creating the aircraft geometry from scratch by only using the Aircraft Library is challenging as there are no tools guiding the user on how to create a stable aircraft with correctly sized and positioned wing and tail. For testing the library in aircraft sizing, a new aircraft with the geometry of the now discontinued Boeing 757-300 was modelled. The motivation for choosing that exact airliner is due to the lack of a direct replacing airliner available at the market [33] [34], and the recent advancements in lighter structural materials make the case for designing a replacement for the Boeing 757 series relevant. Thus, the aircraft sizing process was conducted here by resizing the Boeing 757-300 with using advanced composite materials. The remaining initial design variables and constraints are shown in Tab.3 .4.

**Table 3 .4:** Initial design variables and constraints for the aircraft design to be sized.

Variable	Value
$m_{\text{MTO,des}}$	122,920 kg
$n_{\text{pax}}$	230
$M_{\text{des}}$	0.8
$m_{\text{PL}}$	22,800 kg
$q_{\text{max}}$	0.15 bar
$n_{\text{max}}$	2.5

The limited guidance to the user given by the Aircraft Library when adjusting the parameters for achieving an optimal geometry is compensated by enabling the simulation of any aircraft defined within the allowed parameter space for any detailed flight mission. Given that the range requirement for the new aircraft was to fly from New York to London, the flight data with altitude, velocity and track angle of a real British Airways flight BA112 on 12/21/2019 from New York John F. Kennedy (JFK) to London Heathrow (LHR) from the flight tracking service Flightradar24 was used as the input commands for the autopilot. For modeling the flight to a diversion airport after a missed landing attempt with a required length of 45 minutes [35], the flight data of another British Airways flight BA430 on 02/16/2022 from London Heathrow to Amsterdam Schiphol (AMS) was used. The flight mission with the two flights combined is shown in Fig. 3 .7.

The library is not suitable for modelling neither take-off nor landing at its current status due to the lack of a model for flaps. Thus, minimum values of 1,200 m and 306 km/h were used for altitude and flight speed, respectively. By using the congested London Heathrow as the destination airport, some amount of loitering emerged conveniently into the flight mission prior to landing to LHR.

The altitude given by the Flightradar24 is the calibrated altitude, and thus it corresponds to the geometric altitude used in the library [36]. The velocity given by Flightradar24 however is the ground speed ( $v_{\text{ground}}$ ), that is defined by  $v_{\text{ground}} = v_{\text{tot}} \cos |\gamma|$ , where  $\gamma$  is the flight path angle. Thus, the  $v_{\text{tot}}$  command given to autopilot was actually slightly smaller than the  $v_{\text{tot}}$  of the modelled British Airways flights during climbs and descends.

The track angle values given by Flightradar24 were originally in the range between  $0^\circ$  and  $360^\circ$ . However, the autopilot currently cannot tell the aircraft for example to turn right from a track angle of  $359^\circ$  to  $1^\circ$  or to turn left from  $1^\circ$  to  $359^\circ$  but rather tell the aircraft to turn  $358^\circ$  instead of  $2^\circ$  in both cases. Therefore, the track angles were converted into cumulative rotation angles measured from the initial track angle, and consequently the track angles shown in Fig. 3 .7 have values below  $0^\circ$  and above  $360^\circ$ .

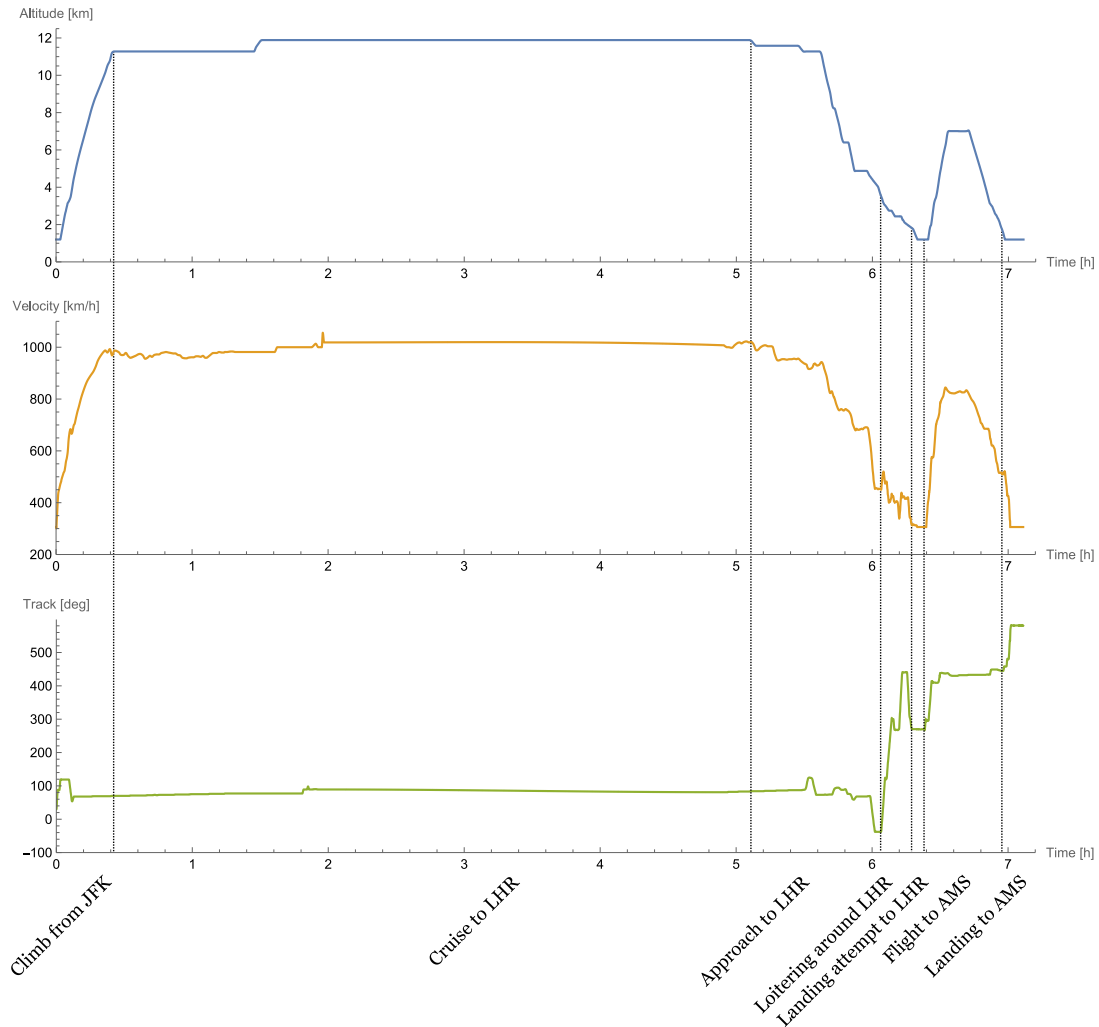


Figure 3.7: Mission profile from JFK to LHR and to diversion airport AMS.

The suggested aircraft sizing flowchart to be followed with the Aircraft Library is shown in Fig. 3.8, and it is adjusted to the functionalities of the library. The first four tasks of the flowchart are the ones earlier described in this section. The simulation of the aircraft design with the set flight mission is followed by four consecutive decisions to check if the aircraft is controllable with the autopilot, flying performance, convergence of  $m_{MTO}$  and if the constraints are satisfied. If any of the checks fails, the suggested corrections are to be followed after which the mission is simulated again, and this is repeated until all checks are satisfied.

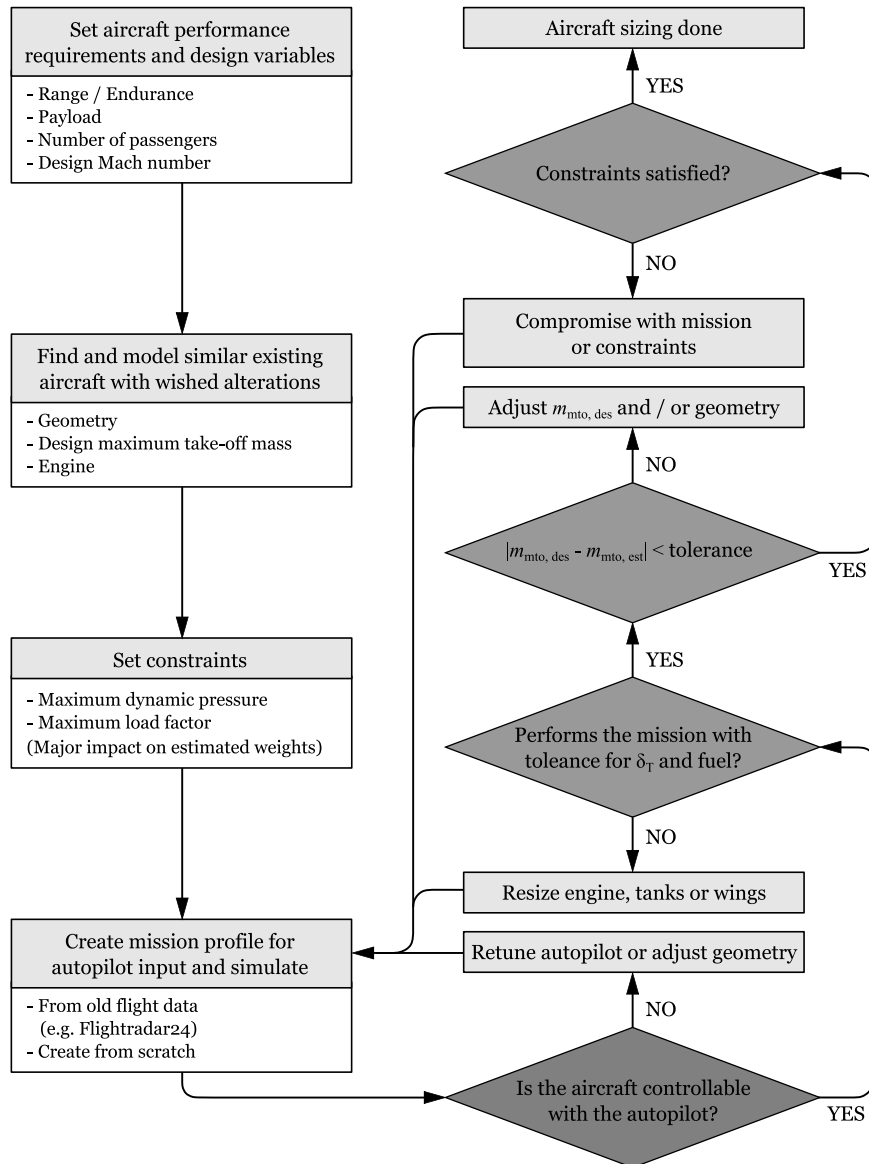


Figure 3.8: Suggested aircraft sizing flowchart to be used with the Aircraft Library.

### 3.8 Verification and Validation

The verification of the model was conducted in terms of the numerical methods used in the solver during simulations. Wolfram System Modeler uses by default the Differential/Algebraic System Solver (DASSL), which is a variable step size and variable order solver. All simulation results in this work are obtained using DASSL with a tolerance of  $1 \text{ e-}6$ . Another variable step size and variable order solver available in Wolfram System Modeler is CVODES. The verification was done by testing different tolerance values with DASSL and CVODES and by changing step sizes with a fixed step size solver that uses Heun's method. [37]

The output data of the simulated flight mission used in the aircraft sizing, including aircraft total mass ( $m_{\text{tot,ac}}$ ), altitude, flight speed and track angles during the entire flight, was used in the verification. The output data was sampled with 1 s intervals, and the results with the altered solver parameters were compared against the results with the used DASSL solver with the tolerance of  $1 \text{ e-}6$ .

The model was validated in terms of the obtained mass and aerodynamic properties. The lift and drag coefficients of the entire aircraft were compared against the results from USAF DATCOM Digital program for few example aircrafts in two different flight conditions with varying velocities and flight altitudes such that also results with different angles of attack would be obtained.

In order to get relevant data output for validating the modelled mass properties, the weights of each component were summed to get the total mass of the aircraft. Additionally, the CG location was solved for the entire aircraft with the estimated component CG locations and their weights. The moments of inertia for the entire aircraft were solved by parallel axis theorem with the simplification of considering the main wing and horizontal tail frames being parallel to the aircraft body frame, and thus ignoring the rotations around dihedral and incidence angles. The products of inertia for the entire aircraft were solved by summing the products of component weights and coordinates:

$$\begin{aligned}
 I_{xy} = I_{yx} &= \sum_{c=1}^N m_c x_c y_c \\
 I_{xz} = I_{zx} &= \sum_{c=1}^N m_c x_c z_c \\
 I_{yz} = I_{zy} &= \sum_{c=1}^N m_c y_c z_c
 \end{aligned} \tag{3 .87}$$

For non electric aircraft, the weight of the entire aircraft is changing over time as the fuel tank weights decrease thus also changing the inertia tensor and shifting the aircraft CG.



## 4 Results

In this chapter, the results of the work are presented. The only presentable results of the work are the cases when the Aircraft Library is applied, i.e. the results of the validation and the use of the model in aircraft sizing.

### 4.1 Sizing

For checking the first condition in the aircraft sizing flowchart in Fig. 3.8 on whether the aircraft is controllable with the autopilot, the plots of interest are altitude, velocity and track angle against the respective command signals from the autopilot. However, for the studied case the aircraft followed the commands well enough for the trajectory variables to be indistinguishable from their respective commands, shown in Fig. 3.7, and thus those plots are omitted here.

For the second check on how much the aircraft burns fuel and on what position the throttle is during the mission, the fuel level as a fraction of the total tank volume and throttle demand from the autopilot are shown in Fig. 4.1. During the aircraft sizing iteration, the tanks were resized such that the fuel level would be 10 % at the end of the mission. By adjusting the tank size and  $m_{MTO,des}$  simultaneously during the iteration, the difference of the estimated maximum take-off mass ( $m_{MTO,est}$ ) to  $m_{MTO,des}$  eventually converged to as low as 0.08 % with little effort. The resulting  $m_{MTO,est}$  reduced to 85,930 kg from the initial  $m_{MTO,des}$  of 122,920 kg. The fuel capacity was 23,360 kg of which 20,869 kg was burned during the mission. The throttle demand from the autopilot rarely hits to full throttle, and at cruise altitude the throttle demand from the autopilot is well below 80 %, and thus the originally set  $T_{static}$  of 192 kN found in Boeing 757-300 [38] was deemed appropriate.

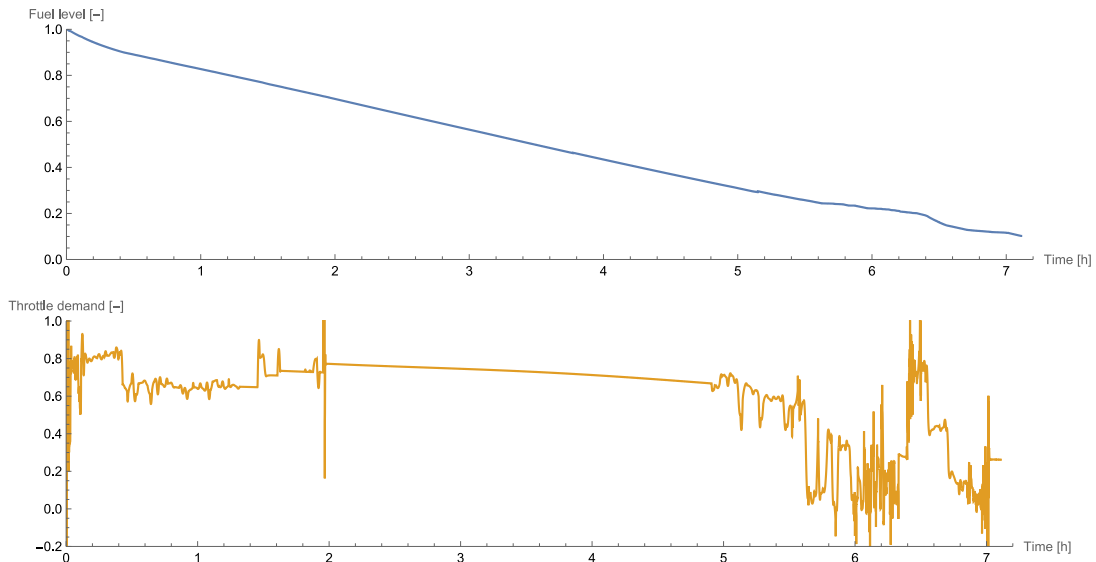


**Figure 4.1:** Fuel level as a fraction of the total tank volume and demand for throttle from autopilot.

Figure 4.2 shows the values for the constrained variables of dynamic pressure and load factor with their set limits. The original limit for  $q$  of 0.15 bar was raised to 0.18 bar during the iteration process to allow the maximum experienced  $q$  of 0.178 bar, which naturally had an increasing effect on  $m_{MTO,est}$ . The load factor had a large margin to the set limit of 2.5. However, the simulated flight mission is lacking any extreme maneuvering situation, and thus the limit for the load factor was not decreased.

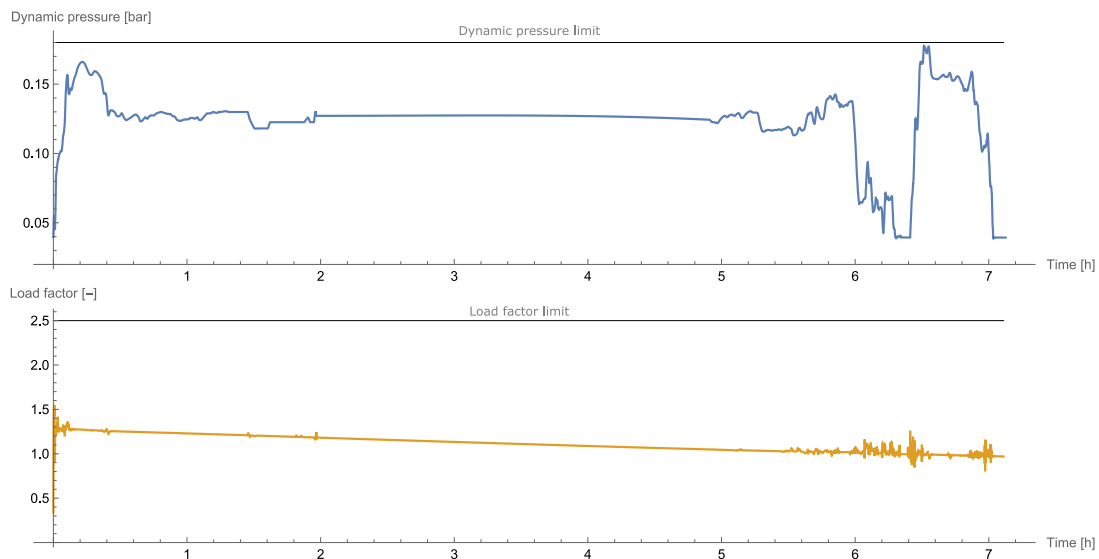


**Figure 4.2:** Constrained variables of dynamic pressure and load factor with their limits.

## 4.2 Verification and Validation

The verification results are presented as the deviations of the total mass and flight trajectory variables during the simulated flight mission from the values using DASSL solver with a tolerance of  $1 \text{ e-}6$  when adjusting the solver parameters. The tolerances used with the variable step size solver range from  $1 \text{ e-}4$  to  $1 \text{ e-}8$ . The fixed time step solver using Heun's method was tested with the step sizes of 0.05 s and 0.01 s. As the magnitude of the deviations of all variables was extremely small, and thus totally indistinguishable from plots, their values are shown quantitatively in Tab. 4.1 by mean squared errors and maximum absolute deviations during the entire simulated flight mission described in Sec. 3.7.

**Table 4.1:** Deviations from the obtained aircraft total mass and flight trajectory variables using DASSL solver with a tolerance of  $1 \text{ e-}6$ .

Mean squared error [%]							
	H 0.05 s	H 0.01 s	C 1 e-4	C 1 e-6	C 1 e-8	D 1 e-4	D 1 e-8
$m_{\text{tot,ac}}$	3.80	2.40 e-5	0.02	1.62 e-5	1.37 e-5	0.08	2.03 e-5
$h$	1.01	1.77 e-6	3.42 e-4	1.89 e-6	1.77 e-6	6.29 e-3	1.77 e-6
$v_{\text{tot}}$	0.04	2.72 e-9	9.02 e-7	4.23 e-10	1.37 e-10	8.91 e-7	1.32 e-10
$track$	6.71 e-4	2.79 e-8	5.63 e-5	2.56 e-8	2.71 e-8	4.38 e-4	2.74 e-8

Maximum absolute deviation							
	H 0.05 s	H 0.01 s	C 1 e-4	C 1 e-6	C 1 e-8	D 1 e-4	D 1 e-8
$m_{\text{tot,ac}}$ [kg]	1.22	1.01 e-3	-0.02	1.21 e-3	8.92 e-4	-0.08	1.30 e-3
$h$ [m]	-5.08	-4.57 e-3	-0.08	-4.58 e-3	-4.57 e-3	0.18	-4.56 e-3
$v_{\text{tot}}$ [km h <sup>-1</sup> ]	-3.36	1.16 e-3	-0.01	-3.40 e-4	1.52 e-4	-0.01	1.52 e-4
$track$ [deg]	0.17	4.31 e-4	-0.03	-4.69 e-4	4.23 e-4	-0.06	4.29 e-4

H = Heun's Method, C = CVODES, D = DASSL

Three aircraft were chosen to be used for validation. Choosing Boeing 737-800, the most sold airliner of all-time [39] [40], made it easy to find data of its properties for comparison of the simulation results. The other two aircraft represent different propulsion types and sizes: Saab 2000, a regional turboprop airliner and an electric general aviation aircraft design that was the result of a previous project course on aircraft conceptual design and thereby the properties of which were well known and tested with other tools.

Table 4.2 shows the comparison of the obtained  $C_D$  and  $C_L$  of the entire aircraft between the USAF DATCOM Digital Program and the Aircraft Library for the three aircraft in a stable flight in lower and higher altitudes that are relevant to each aircraft. The Aircraft Library underestimates both coefficients, especially with higher  $\alpha$  values. The only exception to this is the lift coefficient of Saab 2000 at high altitude where the library overestimates its value.

**Table 4 .2:** Validation of the aerodynamic coefficients against USAF DATCOM Digital Program results.

<b>Electric General Aviation Aircraft Design</b>						
<b>h [m]</b>	<b>M [-]</b>	<b><math>\alpha</math> [deg]</b>	<b>Coefficient</b>	<b>DATCOM</b>	<b>AC Library</b>	<b>Difference</b>
3,000	0.15	2.81	$C_D$ [-]	0.022	0.019	-12.8 %
			$C_L$ [-]	0.42	0.40	-6.2 %
100	0.1	5.63	$C_D$ [-]	0.035	0.029	-18.8 %
			$C_L$ [-]	0.69	0.63	-8.8 %

<b>Saab 2000</b>						
<b>h [m]</b>	<b>M [-]</b>	<b><math>\alpha</math> [deg]</b>	<b>Coefficient</b>	<b>DATCOM</b>	<b>AC Library</b>	<b>Difference</b>
9,000	0.6	1.49	$C_D$ [-]	0.027	0.025	-7.3 %
			$C_L$ [-]	0.42	0.46	9.9 %
1,000	0.3	3.38	$C_D$ [-]	0.038	0.033	-12.2 %
			$C_L$ [-]	0.74	0.64	-14.0 %

<b>Boeing 737-800</b>						
<b>h [m]</b>	<b>M [-]</b>	<b><math>\alpha</math> [deg]</b>	<b>Coefficient</b>	<b>DATCOM</b>	<b>AC Library</b>	<b>Difference</b>
10,000	0.6	6.91	$C_D$ [-]	0.059	0.046	-22.6 %
			$C_L$ [-]	0.98	0.73	-24.8 %
1,000	0.3	8.49	$C_D$ [-]	0.076	0.059	-22.0 %
			$C_L$ [-]	1.14	0.86	-24.3 %

The comparison of the mass properties between the best available data for known values of the aircraft and their estimated counterparts in the library are shown in Tab. 4 .3. For comparing the total masses, the maximum landing masses ( $m_{ML}$ ) instead of  $m_{MTO}$  were used as the loading condition of which the moments of inertia and the xz-product of inertia were given in the different sources is not known, and the aim was to have all the mass properties in somewhat comparable conditions. To estimate the maximum landing mass and inertia tensor values from the Aircraft Library, the mass properties after one hour of flight were used. For the electric aircraft, all mass properties are naturally constant.

The most reliable and accurate data for comparing the obtained estimated mass properties with were found for the maximum landing masses where also the errors of the estimated values were the smallest. However, the inertia tensor values of Boeing 737-800 are not from a reliable source, and for Saab 2000 that data was entirely unavailable but the values of ATR-72 were used for the comparison instead. Consequently, the error of the estimated inertia tensor values are larger but still well in the same order of magnitude with the exception of the  $I_{xz}$  values. The error in  $I_{xz}$  values is still tolerable as its order of magnitude with respect to the  $I_{xx}$ ,  $I_{yy}$  and  $I_{zz}$  is still correct.

Table 4.3: Validation of the mass properties against known values.

<b>Electric General Aviation Aircraft Design</b>			
<b>Mass property</b>	<b>Known</b>	<b>AC Library</b>	<b>Difference</b>
$m_{ML}$ [kg]	595	561	-5.7 %
$I_{xx}$ [kg m <sup>2</sup> ]	630	381	-39.5 %
$I_{yy}$ [kg m <sup>2</sup> ]	797	844	5.9 %
$I_{zz}$ [kg m <sup>2</sup> ]	1,304	1,193	-8.5 %
$I_{xz}$ [kg m <sup>2</sup> ]	242	7	-97.1 %
$x_{CG} / c_{mean,w}$ [-]	15.0 %	50.3 %	35.3 pp

<b>Saab 2000</b>			
<b>Mass property</b>	<b>Known</b>	<b>AC Library</b>	<b>Difference</b>
$m_{ML}$ [kg]	22,000 [41]	20,690	6.0 %
$I_{xx}$ [kg m <sup>2</sup> ]	289,900* [42]	288,633	-0.4 %
$I_{yy}$ [kg m <sup>2</sup> ]	298,400* [42]	430,758	5.9 %
$I_{zz}$ [kg m <sup>2</sup> ]	573,600* [42]	711,879	-14.9 %
$I_{xz}$ [kg m <sup>2</sup> ]	n/a	4,436	n/a
$x_{CG} / c_{mean,w}$ [-]	n/a	22.0 %	n/a

\* ATR-72 value.

<b>Boeing 737-800</b>			
<b>Mass property</b>	<b>Known</b>	<b>AC Library</b>	<b>Difference</b>
$m_{ML}$ [kg]	65,317 [43]	63,584	-2.7 %
$I_{xx}$ [kg m <sup>2</sup> ]	1,866,711 [43]	1,318,345	-29.4 %
$I_{yy}$ [kg m <sup>2</sup> ]	3,394,953 [43]	3,126,650	-7.9 %
$I_{zz}$ [kg m <sup>2</sup> ]	5,097,558 [43]	4,338,608	-14.9 %
$I_{xz}$ [kg m <sup>2</sup> ]	149,140 [44]	75,174	-49.6 %
$x_{CG} / c_{mean,w}$ [-]	24.0 % [45]	29.0 %	5 pp



## 5 Discussion

### 5.1 Method

The methodology is discussed in this section in the same order as it was presented in Chapter 3. Additionally the suggestion for future improvements to the library are presented in this section in their respective subsections.

#### 5.1.1 Autopilot

The autopilots for different aircraft type were arbitrarily tuned by hand through trial and error until a satisfactory performance was achieved. This definitely left the autopilots far from being optimised for any objective. Optimising the autopilots for example to minimise fuel consumption would indeed be an interesting future improvement to the model. Nevertheless, the autopilots showed robust performance with the current gains in terms of controlling aircraft in different flight conditions and with minor changes in the aircraft parameters. The mission definition could also be done on a higher level with an added route planner algorithm translating given scheduled waypoint coordinates into track angle, altitude and flight speed commands.

#### 5.1.2 Fuel Consumption

Currently the  $TSFC$  and  $BSFC$  values are input as constant parameters for the engines despite their values being a function of altitude, velocity and thrust for  $TSFC$  and torque load, engine rotational speed and altitude for  $BSFC$  [46][47]. Thus, creating a map for  $TSFC$  and  $BSFC$  would further improve the fidelity of the fuel consumption models. Furthermore, the  $\eta_{prop}$  and  $\eta_{mech}$  efficiencies that are used for electric, piston and turboprop engines, are constants, and thus the propulsion model could be improved by creating maps for both efficiency parameters.

#### 5.1.3 Algebraic and Statistical Relations Between Geometry and Aerodynamics

The relations between the aerodynamics and the aircraft geometry are all taken from one single source for each relation used in this work despite a number of different methods available in the literature for most relations. Hence, the used methodology could be

diversified by using more sources per relation and either use the average values of the different sources or let the user choose between them.

The only aerodynamic relations created by the author, namely the stall behavior of  $C_D$  and  $C_L$  of the main wing and horizontal tail and the effect of  $\alpha$  to  $C_{D,fus}$ , despite being vaguely supported by sources from the literature or not being thoroughly tested, it is undoubtedly better than having no such models at all. Though the stall is currently modelled with positive  $\alpha$  values only, thereby a model for stall towards  $\alpha = -90^\circ$  is still required to make the stall model complete.

When it comes to adjusting the geometry of the aircraft, the chosen coordinate system with the origin in the middle of the fuselage together that the most of the component coordinates are input as absolute distance to the origin is certainly not the most convenient. Furthermore, the tail x-coordinates are to be input as an absolute distance from the  $c_{mean,w}$  leading edge, as shown in Fig. 5.1. In order to ease the adjustments in the geometry, the coordinate system should be consolidated to having one reference point and, additionally, change the longitudinal coordinates of the components into fractions of the fuselage length.

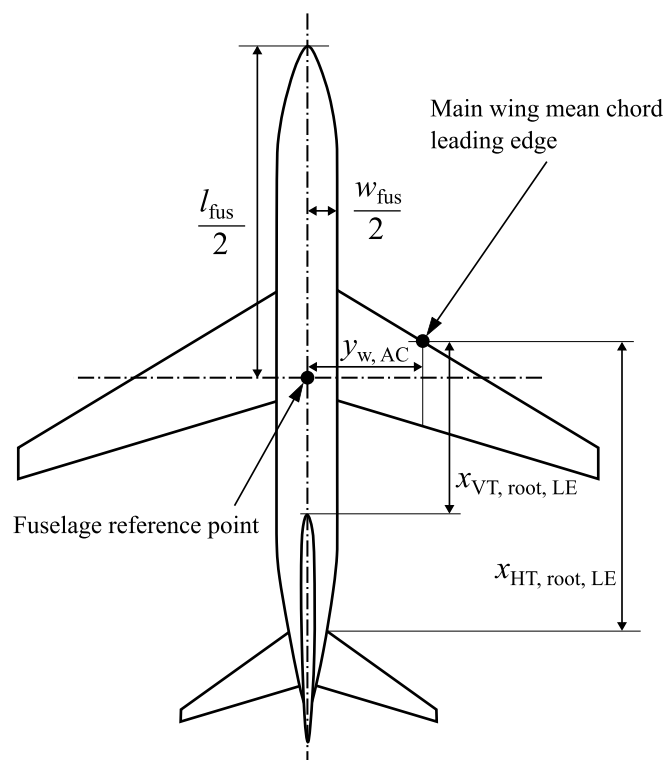


Figure 5.1: Fuselage reference point and  $c_{mean,w}$  leading edge which is used to define the position of the tail.

#### 5.1.4 Mass and Inertia

Similarly to the estimation of the aerodynamic coefficient, only one source per each relation was used to estimate the component mass properties based on the aircraft geometry, design variables and engine properties. Therefore, the same suggestion for diversifying the used method as described in Sec. 5.1.3 could be applied for the estimation of mass properties.

The components whose mass properties were the most challenging to estimate were the fuel tanks and thereupon more simplifications were made there. Firstly, the used fuel tank volume estimation method is only intended for larger airliners, and thus may give unrealistic volumes for general aviation aircraft and smaller business jets. However, the user may always use the fudge factor parameter to adjust the tank volume. Moreover, the CG location and

moments of inertia of the wing fuel tanks were estimated with the assumption of constant spanwise tank thickness, and the location of the wing mounted engines has no effect on the tank shape. There are however models available for considering the effect of both factors, that could be implemented to the library.

Currently, the library has no constraints or relations between the fuselage geometry and number or passengers which imposes the user to set a realistic passenger capacity to their aircraft design.

### 5.1.5 Verification and Validation and the Use of the Model in Aircraft Sizing

With the implemented aircraft sizing method, the connection between the aircraft requirements on range and endurance, constraints and the set flight mission is weak. Despite representing a real flight mission of a passenger airliner accurately and with much detail, the used flight mission in the aircraft sizing does not consider any major deviation from a successful flight. As a future improvement to the library, generating a method for creating different flight missions automatically based on the set constraints and requirements would make the output of the sizing process better match the requirements and constraints of the aircraft. Additionally, the evaluation of the flight performance during sizing could be enhanced by generating a flight envelope for the aircraft design.

The robustness of the library in terms of varying numerical solution methods was briefly studied but the robustness in terms of varying any aircraft parameters was not. For validating the estimated aerodynamic coefficients, only one method, yet it being the well established DATCOM Digital Program, was used for obtaining reference values. Due to the limitation of maximum Mach number of 0.6 in DATCOM Digital, the validation of the aerodynamic coefficients in transsonic regime was not conducted.

## 5.2 Results

In this section, the results of the aircraft sizing example and verification and validation are discussed.

### 5.2.1 Aircraft Sizing

At the end of the aircraft sizing process, the tank volume fudge factor was reduced to 0.45, meaning that the used relation for estimating the fuel tank volume tends to overestimate the volume. The overestimation became apparent also during the validation as the fuel tank volume fudge factor was reduced to 0.7 for both Boeing 737-800 and Saab 2000 in order to get their fuel capacities to match their real values.

The throttle demand from the autopilot shows consistency regarding that the  $T_{static}$  was left unchanged from the corresponding value for Boeing 757-300. The throttle demand at times falls below zero, which is a defect currently found in the propulsion model. Negative thrust is currently allowed for simulating the effect of deploying thrust reverser despite the inability to currently model landings, which is the only occasion when using the thrust reverser is relevant.

### 5.2.2 Verification and Validation

With the extremely small obtained deviations when adjusting the numerical solver parameters used in the simulation, it can be concluded that the model is robust when it comes to numerically solving the ordinary differential equations generated in the library. In the validation, the estimated drag coefficients were all in all 10 to 20 % below the DATCOM Digital values, and the difference increased with higher angles of attack. When the  $C_D$  values of the entire aircraft in the model were forced to higher values as  $\alpha$  deviates from 0 to match

the DATCOM Digital values, for example by increasing the  $C_{D,max,fus}$  value, another issue arose with not having enough thrust from the propulsion for the increased drag, despite using the same  $T_{static}$  value as what really was found in the modelled aircraft. Assuming that the DATCOM Digital  $C_D$  results are accurate, one may doubt that the modelling of the propulsion in this work may have minor defects.

The validation of the mass properties showed solid results with the total masses of all the aircraft used in validation. The largest deviations in the mass properties from the reference values were with the  $I_{xz}$  products of inertia. Given their small absolute values with respect to the moments of inertia, their effect in flight dynamics however is eventually negligibly small. The estimated CG locations of the entire aircraft were within reasonable range with the Boeing 737-800 and Saab 2000 but with the electric general aviation aircraft design the CG location was estimated largely off the reference value. Undoubtedly, the CG location of smaller and especially electric aircraft are extremely sensitive to the aircraft geometry, which may excuse the large error. Additionally, the electric general aviation aircraft design was nevertheless well controllable and stable in the simulations.

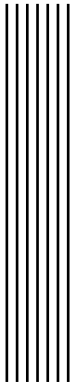


## 6 Conclusions

The Aircraft Library implemented in the Modelica Language using Wolfram System Modeler that was previously capable of simulating a flight of an aircraft with turbofan engines and with known aerodynamic and mass properties in subsonic regime was enhanced to be used as a tool in aircraft conceptual design. The improvements include implementing statistical and empirical relations to estimate the aerodynamic and mass properties of the aircraft design based in its geometry and some selected design variables, the inclusion of air compressibility effects in aerodynamic forces and engine performance and modelling stall for the main wing and horizontal stabilizer up to  $\alpha = 90^\circ$ . Different propulsion types were added with models for calculating fuel consumption resulting in varying mass properties during a flight. Additionally, the autopilots were tuned for four different aircraft types to enable assigning flight missions to different aircraft designs.

The hand-tuned autopilots performed well in controlling the aircraft model in a large spectrum of flight conditions and with small adjustments in the aircraft parameters. The obtained drag coefficients are 10 to 20 % lower than the reference values used for the validation, and forcing them to match the reference values resulted in insufficient engine performance despite the accurately estimated weights and the use of exactly same  $T_{static}$  values as what is found in the real Boeing 737-800 and Saab 2000 aircraft, implying that either the applied drag coefficient or thrust calculations have minor defects.

Overall, the improved Aircraft Library brings a valuable addition to aircraft conceptual design for validating the performance of the aircraft design in terms of aerodynamic properties and stability in any given flight mission considering also the dynamic effects. It however is currently inconvenient for creating the aircraft geometry from scratch or even adjust it as the only feedback for designing the geometry is the trajectory results from the flight simulations.



## Bibliography

- [1] National Oceanic and Atmospheric Administration, National Aeronautics and Space Administration, United States Air Force. *U.S. STANDARD ATMOSPHERE, 1976*. 1976. URL: [https://www.ngdc.noaa.gov/stp/space-weather/online-publications/miscellaneous/us-standard-atmosphere-1976/us-standard-atmosphere\\_st76-1562\\_noaa.pdf](https://www.ngdc.noaa.gov/stp/space-weather/online-publications/miscellaneous/us-standard-atmosphere-1976/us-standard-atmosphere_st76-1562_noaa.pdf).
- [2] Nicolas André. “Sustainable Design of Electric Vertical Take-Off and Landing Aircraft for Urban Air Mobility”. PhD thesis. Technische Universität München, 2022.
- [3] Nicola Cimmino, Sangeeth Saagar Ponnusamy, A Garcia Garriga, and L Mainini. “A modelling and simulation framework for the integrated design of aircraft systems”. In: *Proceedings of the Institution of Mechanical Engineers, Part G: Journal of Aerospace Engineering* 234.10 (2020), pp. 1648–1660.
- [4] Egbert Torenbeek. *Synthesis of subsonic airplane design*. 1st ed. Delft University Press, 1976.
- [5] Daniel P. Raymer. *Aircraft Design: A Conceptual Approach*. 2nd ed. American Institute of Aeronautics and Astronautics, 1992.
- [6] Alexandra Oprea, Robert Hällqvist, Ludvig Knöös Franzén, Magnus Eek, Ingo Staack, and Hampus Gavel. “Connecting system simulation to aircraft concept development”. In: *32nd Congress of the International Council of the Aeronautical Sciences (ICAS 2020), 6-10 September 2021, Shanghai, China*. Sept. 2021.
- [7] Mehdi Ghoreyshi, Adam Jirasek, Steven Brandt, Ryan Osteros, and Russell Cummings. “From spreadsheets to simulation-based aircraft conceptual design”. In: *50th AIAA Aerospace Sciences Meeting including the New Horizons Forum and Aerospace Exposition*. 2012, p. 393.
- [8] Ingo Staack, Raghu Chaitanya Manjula, Patrick Berry, Tomas Melin, Kristian Amadori, Christopher Jouannet, David Lundström, and Petter Krus. “Parametric aircraft conceptual design space”. In: *28th Congress of the International Council of the Aeronautical Sciences (ICAS 2012), 23-28 September 2012, Brisbane, Australia*. 2012.
- [9] David G Hull et al. *Fundamentals of airplane flight mechanics*. Vol. 19. Springer, 2007.
- [10] Robert Nelson. *FLIGHT STABILITY AND AUTOMATIC CONTROL*. 2nd ed. McGraw-Hill, 1998.

- 
- [11] Snorri Gudmundsson. *General Aviation Aircraft Design: Applied Methods and Procedures*. 1st ed. Elsevier, 2014.
- [12] John D. Anderson, Jr. *Aircraft Performance and Design*. 1st ed. WCBMcGraw-Hill, 1999.
- [13] Ahmed F El-Sayed. *Aircraft propulsion and gas turbine engines*. 2nd ed. CRC press, 2017.
- [14] Askin T. Isikveren. "Quasi-analytical modelling and optimisation techniques for transport aircraft design". In: *Department of Aeronautics* (2002), p. 354.
- [15] Pasquale M. Sforza. *Theory of Aerospace Propulsion*. 2nd ed. Elsevier, 2017.
- [16] Eric W. Weisstein. *Cylinder Drag*. 2007. URL: <https://scienceworld.wolfram.com/physics/CylinderDrag.html>.
- [17] C. Ostowari and D. Naik. "Post Stall Studies of Untwisted Varying Aspect Ratio Blades with an NACA 4415 Airfoil Section - Part I". In: *Wind Engineering* 8.3 (1984), pp. 176–194. ISSN: 0309524X, 2048402X. URL: <http://www.jstor.org/stable/43749984>.
- [18] Justin L Petrilli, Ryan C Paul, Ashok Gopalarathnam, and Neal T Frink. "A CFD database for airfoils and wings at post-stall angles of attack". In: *31st AIAA applied aerodynamics conference*. 2013, p. 2916.
- [19] Luca Manni, Takafumi Nishino, and Pierre-Luc Delafin. "Numerical study of airfoil stall cells using a very wide computational domain". In: *Computers Fluids* 140 (2016), pp. 260–269. ISSN: 0045-7930. DOI: <https://doi.org/10.1016/j.compfluid.2016.09.023>. URL: <https://www.sciencedirect.com/science/article/pii/S0045793016302894>.
- [20] C Lindenburg. "Stall coefficients". In: *IEA Symposium on the Aerodynamics of Wind Turbines*. 2000.
- [21] Bjorn Montgomerie. *Drag coefficient distribution on a wing at 90 degrees to the wind*. 1996.
- [22] R. D. Finck. *USAF (United States Air Force) Stability and Control DATCOM (Data Compendium)*. Defense Technical Information Center, 1978.
- [23] Nicolai, Leland M, Carichner, and Grant E. *Fundamentals of aircraft and airship design, Volume 1–Aircraft Design*. American Institute of Aeronautics and Astronautics, 2010.
- [24] Tomáš Vogeltanz. "Application for calculation of mean aerodynamic chord of arbitrary wing planform". In: *AIP Conference Proceedings*. Vol. 1738. 1. AIP Publishing LLC. 2016, p. 120018.
- [25] D Guida and M Minutillo. "Design methodology for a PEM fuel cell power system in a more electrical aircraft". In: *Applied energy* 192 (2017), pp. 446–456.
- [26] R Bojoi, A Cavagnino, A Miotto, A Tenconi, and S Vaschetto. "Radial flux and axial flux PM machines analysis for more electric engine aircraft applications". In: *2010 IEEE Energy Conversion Congress and Exposition*. IEEE. 2010, pp. 1672–1679.
- [27] Ding Ding and Yunfei Zhang. "Improved Fuel Capacity Estimation Method". In: *Journal of aircraft* 47.5 (2010), pp. 1798–1803.
- [28] Hendrik L bberding, Saskia Wessel, Christian Offermanns, Mario Kehrer, Johannes Rother, Heiner Heimes, and Achim Kampker. "From cell to battery system in BEVs: analysis of system packing efficiency and cell types". In: *World Electric Vehicle Journal* 11.4 (2020), p. 77.
- [29] US Department of Transportation, Federal Aviation Administration. *Aircraft Weight and Balance Control*. 1995.
- [30] Jan Roskam. *Airplane Design Part V: Component Weight Estimation*. 5th ed. DARcorporation, 2018.

- [31] StructX. *General Trapezoid - Geometric Properties*. URL: [https://structx.com/Shape\\_Formulas\\_027.html](https://structx.com/Shape_Formulas_027.html). (accessed: 2022-03-21).
- [32] Yage Zheng, Francis G Wagner, Philip H Steele, and Zhendong Ji. "Two-dimensional geometric theory for maximizing lumber yield from logs". In: *Wood and fiber science* 21.1 (1989), pp. 91–100.
- [33] Marisa Garcia. *Why Boeing Should Commit To A New Midsize Airplane Amid 737 MAX Crisis*. 2019. URL: <https://www.forbes.com/sites/marisagarcia/2019/04/29/should-boeing-commit-to-new-797-nma-now-while-addressing-737-max-issues/?sh=56d13e846bd2> (visited on 05/09/2022).
- [34] Edward Russell. *PARIS: A321XLR not a full mid-market solution to United*. 2019. URL: <https://www.flightglobal.com/strategy/paris-a321xlr-not-a-full-mid-market-solution-to-united/133153.article> (visited on 05/09/2022).
- [35] European Aviation Safety Agency. *Annex VI - draft Commission Regulation on Air Operations - OPS*. 2012. URL: <https://www.easa.europa.eu/downloads/9762/en>.
- [36] Flightradar24 AB. *Aviation glossary flight tracking terminology*. 2022. URL: <https://www.flightradar24.com/glossary>.
- [37] Wolfram. *Simulation Center—Experiment Browser*. 2022. URL: <https://reference.wolfram.com/system-modeler/UserGuide/SimulationCenterExperimentBrowser.html> (visited on 06/05/2022).
- [38] Raytheon Technologies Corporation - Pratt Whitney Division. *PW2000 ENGINE*. 2020. URL: <https://prattwhitney.com/products-and-services/products/commercial-engines/pw2000>.
- [39] Boeing. *Orders Deliveries*. 2022. URL: <https://www.boeing.com/commercial/#/orders-deliveries>.
- [40] Airbus. *Orders Deliveries April 2022*. 2022. URL: <https://www.airbus.com/sites/g/files/jlcbta136/files/2022-05/ODs-April-2022-Airbus-Commercial-Aircraft.xlsx>.
- [41] Saab Aircraft Leasing. *SAAB 2000*. 2009. URL: [https://www.saabaircraftleasing.com/prod/datasheets/2000\\_JAR.pdf](https://www.saabaircraftleasing.com/prod/datasheets/2000_JAR.pdf).
- [42] Aviation Safety Council Taipei, Taiwan. *GE 791 Occurrence Investigation Report*. 2002. URL: [https://www.smartcockpit.com/docs/OTHERPROPS\\_ATR72-Inflight\\_Icing\\_and\\_Crash.pdf](https://www.smartcockpit.com/docs/OTHERPROPS_ATR72-Inflight_Icing_and_Crash.pdf).
- [43] Shifu Liu, Jianming Ling, Yu Tian, and Jinsong Qian. "Assessment of aircraft landing gear cumulative stroke to develop a new runway roughness evaluation index". In: *International Journal of Pavement Engineering* (2021), pp. 1–12.
- [44] Michael Soitanen. *Boeing 737-800YV for Flightgear*. 2014. URL: <https://github.com/YV3399/737-800YV/blob/master/737-800YV.xml>.
- [45] Yitao Liu, Zhenbo Yang, Junxiang Deng, and Junjie Zhu. "Investigation of fuel savings for an aircraft due to optimization of the center of gravity". In: *IOP Conference Series: Materials Science and Engineering*. Vol. 322. 7. IOP Publishing. 2018, p. 072018.
- [46] Artur Bensel. *Characteristics of the Specific Fuel Consumption for Jet Engines*. Hamburg: Aircraft Design, Systems Group (AERO), Department of Automotive, and Aeronautical Engineering, Hamburg University of Applied Sciences, 2018.
- [47] JO Kreyer, M Müller, and Thomas Esch. *A map-based model for the determination of fuel consumption for internal combustion engines as a function of flight altitude*. Deutsche Gesellschaft für Luft-und Raumfahrt-Lilienthal-Oberth eV, 2020.



# A Appendices

## A.1 Wing Coordinates

### Main Wing

The main wing origin was set to root quarter chord along the fuselage centreline, as shown in Fig. A .1. The rotations of the wing halves around the angles  $\Gamma_w$  and  $i_w$  (in that order) are applied around the origin.

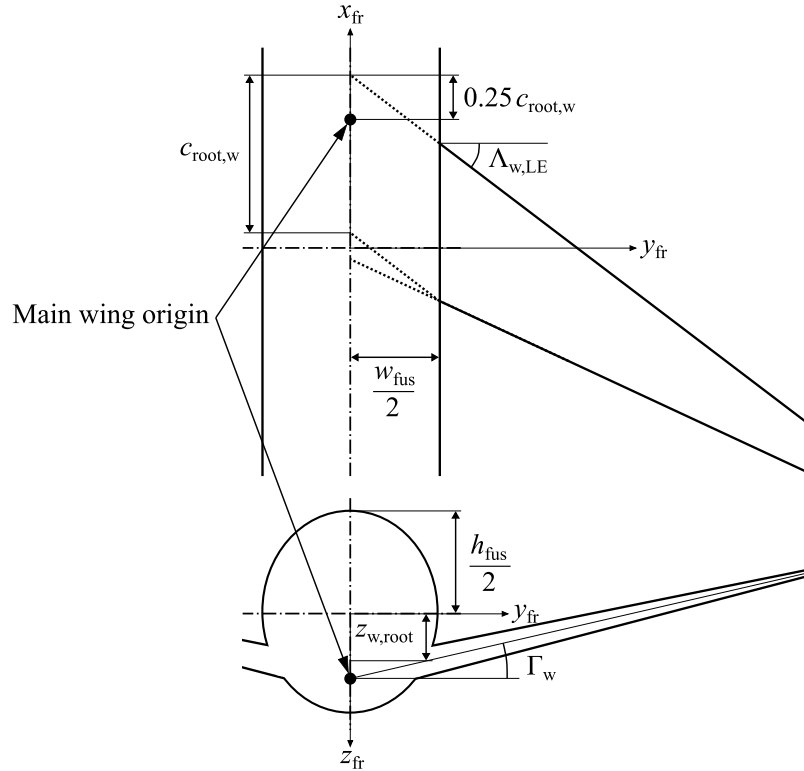


Figure A .1: The position of the main wing origin.

The wing origin coordinates with respect to fuselage reference point are:

$$\begin{aligned} x &: x_{w,\text{root}} + \tan \Lambda_{w,\text{LE}} \frac{w_{\text{fus}}}{2} - \frac{c_{\text{root},w}}{4} \\ y &: 0 \\ z &: z_{w,\text{root}} - \tan \Gamma_w \frac{w_{\text{fus}}}{2} \end{aligned}$$

The CG location was solved for a half wing with respect to main wing origin on a xy-plane parallel to the wing surface after rotations around  $\Gamma_w$  and  $i_w$ . The coordinates for a swept main wing are

$$\begin{aligned} x &: \frac{c_{\text{root},w}}{4} - \tan \Lambda_{w,\text{LE}} \left( 0.35 \frac{b_w}{2} - \frac{w_{\text{fus}}}{2} \right) - 0.5 \left[ \frac{c_{\text{tip},w} - c_{\text{root},w}}{b_w/2 - w_{\text{fus}}/2} \left( 0.35 \frac{b_w}{2} - \frac{w_{\text{fus}}}{2} \right) + c_{\text{root},w} \right] \\ y &: \pm 0.35 \frac{b_w}{2 \cos \Gamma_w}, (+) \text{ for right wing, } (-) \text{ for left wing} \\ z &: 0 \end{aligned}$$

and for an unswept wing

$$\begin{aligned} x &: \frac{c_{\text{root},w}}{4} - \tan \Lambda_{w,\text{LE}} \left( 0.4 \frac{b_w}{2} - \frac{w_{\text{fus}}}{2} \right) - 0.4 \left[ \frac{c_{\text{tip},w} - c_{\text{root},w}}{b_w/2 - w_{\text{fus}}/2} \left( 0.4 \frac{b_w}{2} - \frac{w_{\text{fus}}}{2} \right) + c_{\text{root},w} \right] \\ y &: \pm 0.4 \frac{b_w}{2 \cos \Gamma_w}, (+) \text{ for right wing, } (-) \text{ for left wing} \\ z &: 0 \end{aligned}$$

### Horizontal Tail

The origin of the horizontal tail was set to its aerodynamic centre location on body x-axis and at fuselage centreline on body y-axis. Its coordinates with respect to fuselage reference point are

$$\begin{aligned} x &: x_{w,\text{root}} - \tan \Lambda_{w,\text{LE}} \left( y_{w,\text{AC}} - \frac{w_{\text{fus}}}{2} \right) + x_{w,\text{AC}} - l_{\text{HT}} \\ y &: 0 \\ z &: z_{\text{HT,FRP}} \end{aligned}$$

Horizontal tail CG coordinates with respect to horizontal tail origin on a xy-plane parallel to the horizontal tail surface after a rotation around  $i_{\text{HT}}$  are

$$\begin{aligned} x &: \frac{c_{\text{mean,HT}}}{4} + \tan \Lambda_{\text{HT,LE}} \frac{b_{\text{HT}} - w_{\text{fus,HT}}}{2} \frac{1 + 2 \lambda_{\text{HT}}}{3 + 3 \lambda_{\text{HT}}} - \tan \Lambda_{\text{HT,LE}} \left( y_{\text{HT,CG}} - \frac{w_{\text{fus,HT}}}{2} \right) - 0.42 c_{\text{CG,HT}} \\ y &: 0 \\ z &: 0 \end{aligned}$$

where the y-coordinate of half horizontal tail CG location ( $y_{\text{HT,CG}}$ ) and half horizontal chord length ( $c_{\text{CG,HT}}$ ) at  $y_{\text{HT,CG}}$  are defined as

$$\begin{aligned} y_{\text{HT,CG}} &= 0.38 \frac{b_{\text{HT}}}{2} \\ c_{\text{CG,HT}} &= \frac{2(c_{\text{tip,HT}} - c_{\text{root,HT}})}{b_{\text{HT}} - w_{\text{fus,HT}}} \left( y_{\text{HT,CG}} - \frac{w_{\text{fus,HT}}}{2} \right) + c_{\text{root,HT}} \end{aligned}$$

## Vertical Tail

The origin of the vertical tail was set to its aerodynamic centre location. Its coordinates with respect to fuselage reference point are

$$\begin{aligned} x &: x_{w,\text{root}} - \tan \Lambda_{w,\text{LE}} \left( y_{w,\text{AC}} - \frac{w_{\text{fus}}}{2} \right) + x_{w,\text{AC}} - l_{\text{VT}} \\ y &: 0 \\ z &: z_{\text{VT},\text{root}} - b_{\text{VT}} \frac{1 + 2 \lambda_{\text{VT}}}{3 + 3 \lambda_{\text{VT}}} \end{aligned}$$

Vertical tail CG coordinates with respect to its origin are

$$\begin{aligned} x &: \frac{c_{\text{mean,VT}}}{4} + \tan \Lambda_{\text{VT,LE}} b_{\text{VT}} \frac{1 + 2 \lambda_{\text{VT}}}{3 + 3 \lambda_{\text{VT}}} - \tan \Lambda_{\text{VT,LE}} |z_{\text{VT,CG}}| - 0.42 c_{\text{CG,VT}} \\ y &: 0 \\ z &: b_{\text{VT}} \frac{1 + 2 \lambda_{\text{VT}}}{3 + 3 \lambda_{\text{VT}}} + z_{\text{VT,CG}} \end{aligned}$$

where the z-coordinate of vertical tail CG location with respect to its root chord ( $z_{\text{VT,CG}}$ ) and its chord length ( $c_{\text{CG,VT}}$ ) at  $z_{\text{VT,CG}}$  are defined as

$$\begin{aligned} z_{\text{VT,CG}} &= \left[ -\frac{\min(z_{\text{HT,FRP}} - z_{\text{VT,root}}, 0)}{b_{\text{VT}}} (0.55 - 0.38) + 0.38 \right] (-b_{\text{VT}}) \\ c_{\text{CG,VT}} &= \frac{c_{\text{tip,VT}} - c_{\text{root,VT}}}{b_{\text{VT}}} |z_{\text{VT,CG}}| + c_{\text{root,VT}} \end{aligned}$$

## A .2 Moment of Inertia Estimation for Wings and Fuselage

The moments of inertia for wings and fuselage were estimated through the method presented in USAF DATCOM [22], which presents the equations to be used in imperial units. Here all equation are converted to work with standard SI-units. Additionally, the factors to which values are to be estimated from plots in [22] were estimated here with functions fitted to those plots, and they are integrated to relations shown below.

### Fuselage

The moments of inertia for the fuselage about its CG location were estimated for the structural mass and systems installed onboard and excluding the payload.

#### Fuselage Rolling $I_{xx,fus}$

$$I_{xx,fus} = \frac{S_{wet,fus}^2 [(0.016723 \sqrt{C_{fus}} + 0.00159486) m_{fus} + 0.00159486 m_{sys}]}{l_{fus}^2}$$

#### Fuselage Pitching $I_{yy,fus}$

$$I_{yy,fus} = 0.0265765 S_{wet,fus} \left( \frac{3 C_{fus}}{2\pi l_{fus}} + \frac{\pi l_{fus}}{C_{fus}} \right) \left( 0.986993 - \frac{1.86533 |x_{fus,CG}|}{l_{fus}} \right) (m_{fus} + m_{sys})$$

where  $x_{fus,CG}$  is the fuselage CG x-coordinate with respect to fuselage reference point.

#### Fuselage Yawing $I_{zz,fus}$

$$I_{zz,fus} = I_{xx,fus} + I_{yy,fus}$$

### Main Wing

The moments of inertia were estimated for a half wing about their CG locations. However, similarly to Sec. 3 .4, the weight  $m_w$  used here represents the weight of the entire main wing.

#### Main Wing Rolling $I_{xx,w}$

$$I_{xx,w} = 0.00695416 b_w^2 m_w \left[ \frac{3099.99 c_{root,w} c_{tip,w}}{(39.37 c_{root,w} + 39.37 c_{tip,w})^2} + 1 \right] \\ \times \left\{ 15.8221 \left[ \frac{y_{w,CG} (c_{root,w} + c_{tip,w})}{b_w (c_{root,w} + 2c_{tip,w})} \right]^{1.1} - 0.988158 \right\}$$

where  $y_{w,CG}$  is the y-coordinate of half wing CG with respect to the main wing origin, as defined in Appendix A .1.

#### Main Wing Pitching $I_{yy,w}$

$$I_{yy,w} = 0.000205979 \left[ \frac{0.18375 m_w (-C_a^3 + C_b^3 + C_b^2 C_c + C_b C_c^2 + C_c^3)}{-C_a + C_b + C_c} \right. \\ \left. - \frac{0.1225 m_w (-C_a^2 + C_b^2 + C_b C_c + C_c^2)^2}{(-C_a + C_b + C_c)^2} \right]$$

where  $C_a$  is the smallest,  $C_b$  is the intermediate and  $C_c$  is the largest of the following lengths:

$$39.37 c_{root,w} ; 19.685 \tan \Lambda_{w,LE} b_w ; 39.97 c_{tip,w} + 19.685 \tan \Lambda_{w,LE} b_w$$

### Main Wing Yawing $I_{zz,w}$

$$I_{zz,w} = I_{xx,w} + I_{yy,w}$$

### Horizontal Tail

The moments of inertia for horizontal tail were estimated for the entire horizontal tail about its CG location.

### Horizontal Tail Rolling $I_{xx,HT}$

$$I_{xx,HT} = \frac{0.0417249 b_{HT}^2 m_{HT} (c_{root,HT} + 3 c_{tip,HT}) \left[ \frac{2.2747(c_{root,HT} + c_{tip,HT})}{c_{root,HT} + 2 c_{tip,HT}} - 1.06793 \right]}{c_{root,HT} + c_{tip,HT}}$$

### Horizontal Tail Pitching $I_{yy,HT}$

$$I_{yy,HT} = 0.000225903 \left[ \frac{0.3675 m_{HT} (-C_a^3 + C_b^3 + C_b^2 C_c + C_b C_c^2 + C_c^3)}{-C_a + C_b + C_c} - \frac{0.245 m_{HT} (-C_a^2 + C_b^2 + C_b C_c + C_c^2)^2}{(-C_a + C_b + C_c)^2} \right]$$

where  $C_a$  is the smallest,  $C_b$  is the intermediate and  $C_c$  is the largest of the following lengths:

$$39.37 c_{root,HT} ; 19.685 \tan \Lambda_{HT,LE} b_{HT} ; 39.37 c_{tip,HT} + 19.685 \tan \Lambda_{HT,LE} b_{HT}$$

### Horizontal Tail Yawing $I_{zz,HT}$

$$I_{zz,HT} = I_{xx,HT} + I_{yy,HT}$$

### Vertical Tail

The moments of inertia for vertical tail were estimated for the exposed vertical tail about its CG location.

### Vertical Tail Rolling $I_{xx,VT}$

$$I_{xx,VT} = 0.0556333 b_{VT}^2 m_{VT} \left[ \frac{3099.99 c_{root,VT} c_{tip,VT}}{(39.37 c_{root,VT} + 39.37 c_{tip,VT})^2} + 1 \right] \times \left\{ 7.38128 |z_{VT,CG}|^{1.1} \left[ \frac{c_{root,VT} + c_{tip,VT}}{b_{VT}(c_{root,VT} + 2 c_{tip,VT})} \right]^{1.1} - 0.988158 \right\}$$

### Vertical Tail Pitching $I_{yy,VT}$

$$I_{yy,VT} = I_{xx,VT} + I_{zz,VT}$$

### Vertical Tail Yawing $I_{zz,VT}$

$$I_{zz,VT} = 0.000225903 \left[ \frac{0.3675 m_{VT} (-C_a^3 + C_b^3 + C_b^2 C_c + C_b C_c^2 + C_c^3)}{-C_a + C_b + C_c} - \frac{0.245 m_{VT} (-C_a^2 + C_b^2 + C_b C_c + C_c^2)^2}{(-C_a + C_b + C_c)^2} \right]$$

where  $C_a$  is the smallest,  $C_b$  is the intermediate and  $C_c$  is the largest of the following lengths:

$$39.37 c_{root,VT} ; 39.37 \tan \Lambda_{VT,LE} b_{VT} ; 39.37 c_{tip,VT} + 39.37 \tan \Lambda_{VT,LE} b_{VT}$$